UNIVERSITY OF CALIFORNIA
RIVERSIDE

ZnO Nanowire Array-Based Optoelectronic Devices

A Dissertation submitted in partial satisfaction
of the requirements for the degree of

Doctor of Philosophy

in

Electrical Engineering

by

Guoping Wang

August 2011

Dissertation Committee:
Dr. Jianlin Liu, Chairperson
Dr. Alexander N. Korotkov
Dr. Sheldon Tan

The Dissertation of Guoping Wang is approved:

_____

_____

_____

Committee Chairperson

University of California, Riverside

Acknowledgements

First of all, I appreciate my supervisor Prof. Jianlin Liu for his continuously financial support, the lab facilities and the great freedom in research, without which I cannot complete my PhD study. Also I thank to the funding agents (NSF, ARO-YIP, DOE) for supporting my research work. Secondly, I would like to thank Prof. Alexander N. Korotkov and Prof. Sheldon Tan for serving as my final dissertation defence committee members. I also thank all the past and present members of the QSL laboratory who gave me help during my PhD research and study: Mr. Sheng Chu, Mr. Mario Olmedo, Mr. Lin Li, Ms. Huimei Zhou, Ms. Jieying Kong, Mr. Zheng Zuo, Mr. Ning Zhan, Mr. Jingjian Ren. Mr. Jian Huang, Ms. Zonglin Li, Mr. Steve Zhang and Mr. Monzur Morshed.

Finally, I would like to thank to my family. Without their love, encouragement and support, I couldn't finish my Ph. D. study smoothly.

Dedication

To my parents and Jian Kaiqun

ABSTRACT OF THE DISSERTATION

ZnO Nanowire Array-Based Optoelectronic Devices

by

Guoping Wang

Doctor of Philosophy, Graduate Program in Electrical Engineering
University of California, Riverside, August 2011
Dr. Jianlin Liu, Chairperson

ZnO nanowire array-based optoelectronic devices are discussed in this dissertation. ZnO has a wide band gap of 3.37 eV and a large exciton binding energy of 60 meV at room temperature, which make it a promising candidate for optoelectronic devices such as blue-light emitting diodes, ultraviolet laser diodes and photodiodes. Recently, there have been tremendous interests in ZnO nanowire arrays. It is well known that one of the biggest challenges toward good ZnO-based optoelectronic devices is the difficulty of reliably fabricating p-type ZnO due to the self-compensating effect from native defects (for example, oxygen vacancy V_o and zinc interstitial Zn_i) and/or H incorporation. There has already been a great deal of efforts on the fabrication of p-type ZnO films by doping group I (Na, Ag) and group V elements (N, P, As, Sb) as p-type dopants. In contrast, there have been only a few reports on p-type ZnO nanowires (doped with N, P and Na). Recently, researchers are interested in developing optoelectronic devices based on ZnO nanowires such as biosensors, ultraviolet detectors, ultraviolet light emitting diodes and electrically driven nanowire lasers. The growth of p-type ZnO nanowires with good stability will be an essential step for the applications of nanowires in nanoelectronics and optoelectronics. In this dissertation, first， n-type ZnO nanowire array and its application

have been discussed. ZnO has very high electronic carrier mobility and electron affinity, making it a very possible candidate as an effective dye-sensitized solar cell (DSSC) semiconductor. The great properties of vertically aligned ZnO-nanowire array, such as large surface area and fast electron-transport rate, make it a very promising option for the photoanode of DSSCs. Nanowires provide electrons injected from optically excited dye a direct effective path to collecting electrode via the semiconductor conduction band, offering the potential for much faster charge transport than nanoparticle cells. In order to make homojunctional devices based on ZnO nanowire, a great deal of efforts has been made on the growth of p-type ZnO nanowire. Ag, a group Ib element, was predicted to be an acceptor in ZnO when incorporated into substitutional Zn sites and researchers experimentally demonstrated reliable fabrication of p-type ZnO thin films doped with Ag on sapphire substrate and also demonstrated the possibility of achieving Ag-doped p-type ZnO nanowires. Also Sb as an effective dopant for reproducible p-type ZnO thin films has been shown in our group. In chapter 3 of this dissertation, the synthesis and characterization of single-crystalline Ag-doped p-type ZnO nanowires and also Sb-doped p-type ZnO nanowire arrays have been discussed. In chapter 4 of this dissertation, ZnO homojunction photodiodes based on Sb-doped p-type nanowire array have been discussed. In chapter 5 of this dissertation, LED devices based on Sb-doped p-type nanowire array have been discussed. In chapter 6 of this dissertation, electrically pumped ZnO nanowire-waveguided lasing based on Sb-doped p-type nanowire array has been discussed. In chapter 7, the gain calculation for ZnO has been made and a brief discussion about the

comparison between the calculation results and the experimental results has also been made. In chapter 8, Lists of conclusions are made for this dissertation.

Table of Contents

List of Figures

List of Tables

Chapter One Introduction

Semiconductor ZnO, which has the direct wide band gap of 3.3 eV at 300 K [1], has been studied for many decades. There are three crystal structures of ZnO existing in nature, which are Wurtzite, Zinc-blende and Rock-salt (Fig.1.1). However, Zinc-blende and Rock-salt are in unstable phases. The basic properties of Wurtzite structure ZnO are described in the following table 1. 1. [2]

Property	Value
Lattice parameters at 300 K	
a_0	0.324 95 nm
c_0	0.520 69 nm
a_0/c_0	1.602 (ideal hexagonal structure shows 1.633)
u	0.345
Density	5.606 g/cm^3
Stable phase at 300 K	Wurtzite
Melting point	1975 °C
Thermal conductivity	0.6, 1–1.2
Linear expansion coefficient(/C)	a_0:6.5×10^{-6} c_0:3.0×10^{-6}
Static dielectric constant	8.656
Refractive index	2.008, 2.029
Energy gap	3.4 eV, direct
Intrinsic carrier concentration	$<10^6$ cm^{-3}
Exciton binding energy	60 meV
Electron effective mass	0.24
Electron Hall mobility at 300 K for low n-type conductivity	200 cm^2/V s
Hole effective mass	0.59
Hole Hall mobility at 300 K for low p-type conductivity	5–50 cm^2/V s

Table 1.1 Properties of Wurtzite ZnO [2].

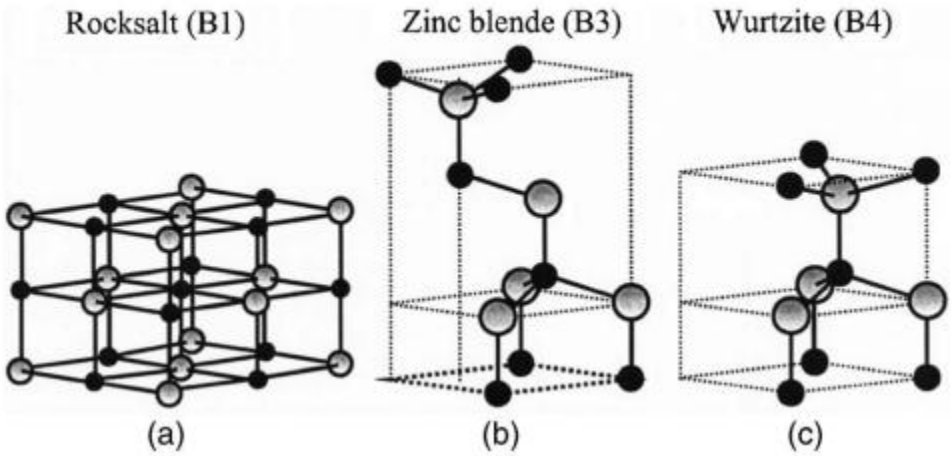

Fig.1.1 Three naturally existing crystal structures of ZnO [3].

Various applications based on ZnO such as gas sensors, surface acoustic wave devices and transparent window for solar cells have been developed [4]. Additionally, increasing interest has been greatly attracted to ZnO because of its optoelectronic properties. The band gap of ZnO of 3.3 eV at room temperature, exactly falling in the blue and ultraviolet region, makes the material a very promising candidate for optoelectronic devices. Because of its large exciton binding energy of 60 meV [5], ZnO has a great potential as an alternative of GaN for laser and LED applications. By doping ZnO with Cd or Mg, its band gap can be tuned in a large range.

In order to fabricate optoelectronic devices based on ZnO, the key step is to develop a reliable ZnO technology with the potential of fabricating *p*-type ZnO. *N*-type ZnO can be easily accomplished by doping with Al, Ga or In. Even excess Zn during the growth process can unintentionally result in *n*-type ZnO due to extra electrons contributed from Zn. As well known, the high "intrinsic" *n*-type conductivity of nominally undoped ZnO,

which is usually thought to originate from point defects, is the biggest major obstacle in achieving *p*-type ZnO. An electron concentration of typically $10^{17}cm^{-3}$ has been observed even on the high-quality bulk ZnO material, which is mainly due to the shallow donors in ZnO, such as hydrogen and structural defects (for example, oxygen vacancy V_o and zinc interstitial Zn_i) [6]. There has already been a great deal of efforts on the fabrication of p-type ZnO by doping group V elements, such as N, P, As. [7-9] Previously, our group showed that Sb, another group V element, is an effective dopant for reproducible p-type ZnO thin films [10] on Si and sapphire substrates. Sb is expected to introduce acceptors in ZnO. Sb-doped *p*-type ZnO with a resistivity of 8×10^{-3} Ω-cm, a hole mobility of 1.5 cm^2/V-s and an acceptor concentration of $5\times10^{20}cm^{-3}$ by excimer laser irradiation has experimentally demonstrated by T. Aoki et al. [11] Theoretically, guided by strain relief and Coulomb interaction, Sukit et al. [12], explain the microscopic origin of Sb-doped *p*-type ZnO. They found that the origin of the p-type conductivity of the Sb-doped ZnO is from the shallow acceptors formed by substitutional Sb_{Zn} simultaneously connecting two Zn vacancies [12], which means Sb_{Zn}-$2V_{Zn}$ complex represents a new class of low energy defects with shallow acceptor levels with both low formation energy, $\Delta H_f(0)$ = 2.0 eV, and low ionization energy, $\varepsilon(0/-)$ = 0.16eV.

Heterojunction [13] and homojunction [14] light emitting diodes, laser diodes as well as photodiodes based on Sb-doped p-type ZnO thin films were achieved in our group. Recently, there have been tremendous interests in ZnO nanowire arrays. Although heterojunction optoelectronic devices [15-17] have been fabricated based on vertically aligned ZnO nanowire arrays, there still lacks the homojunction type devices based on p-

type nanowire array/n-type ZnO film. Sb-doped p-type ZnO nanowires, have clearly improved the potential of the practical applications in nanowire-based LED, laser and photodetector devices.

In this dissertation, the author has explored new approaches for p-type doping of ZnO nanowires using Sb and Ag and nanowire arrays using Sb. In addition, detailed understanding of devices such as photodiodes, LED and laser diodes based on Sb-doped p-type nanowire array/n-type ZnO film is given in the hope of further facilitating the research progress in the ZnO homojunction devices.

In brief, this dissertation consists of the following eight chapters.

Chapter 1: Introduction. The basic properties of ZnO are presented. The current challenge for ZnO homojunction devices especially for ZnO nanowire devices is discussed, which serves as the background for the present work.

Chapter 2: The growth of n-type vertical ZnO nanowire array and the application in dye-sensitized solar cell is discussed.

Chapter 3: Synthesis of Ag-doped p-type ZnO nanowires and Sb-doped p-type ZnO nanowire array.

Chapter 4: ZnO homojunction photodiodes based on Sb-doped p-type nanowire array and n-type film for ultraviolet detection.

Chapter 5: ZnO homojunction LEDs based on Sb-doped p-type nanowire array and n-type film.

Chapter 6: Electrically pumped waveguide lasing from ZnO nanowires.

Chapter 7: Lasing mechanism and gain calculation of ZnO.

Chapter 8: Conclusion

References

1. E. O. Kane, Phys. Rev. B **18**, 6849 (1978).
2. S. J. Pearton, D. P. Norton, K. Ip, Y. W. Heo, T. Steiner, *Superlattices and Microstructures* .3 (2003) 34.
3. Ü. Özgür, Ya. I. Alivov, C. Liu, A. Teke, M. A. Reshchikov, S. Doğan, V. Avrutin, S.-J. Cho, and H. Morkoç. JOURNAL OF APPLIED PHYSICS 98 (2005) 041301.
4. A. Waag, Th. Gruber, K. Thonke, R. Sauer, R. Kling, C. Kirchner and H. Ress, *J. alloys and compounds.* 77 (2004) 371.
5. C. Klingshirn,Phys. Status. Solidi. B **244**, 3027(2007).
6. C. G. Van de Walle, Phys. Rev. Lett. **85**, 1012 (2000).
7. D. K. Hwang, H. S. Kim, J. H. Lim, J. Y. Oh, J. H. Yang, S. J. Park, K. K. Kim, D. C. Look, and Y. S. Park, Appl. Phys. Lett. **86**, 151917 (2005).
8. K. K. Kim, H. S. Kim, D. K. Hwang, J. H. Lim, and S. J. Park, Appl. Phys. Lett. **83**, 63 (2003).
9. T. S. Jeong, M. S. Han, C. J. Youn, and Y. S. Park, J. Appl. Phys. **96**, 175 (2004).
10. F. X. Xiu, Z. Yang, L. J. Mandalapu, D. T. Zhao, and J. L. Liu, Appl. Phys. Lett. **87**, 152101 (2005).
11. T. Aoki, Y. Hatanaka, and D. C. Look, Appl. Phys. Lett., **76**, 3257 (2000).
12. Sukit Limpijumnong, S. B. Zhang, Su-Huai Wei, and C. H. Park, Phy. Rev. Lett. **92,**16 (2004).
13. L. J. Mandalapu, F. X. Xiu, Z. Yang, D. T. Zhao, and J. L. Liu, Appl. Phys. Lett. **88**, 112108 (2006).
14. L. J. Mandalapu, Z. Yang, F. X. Xiu, D. T. Zhao, and J. L. Liu, Appl. Phys. Lett. **88**,

092103 (2006).

15. C. H. Chen, S. J. Chang, S. P. Chang, M. J. Li, I. C. Chen, T. J. Hsueh, and C. L. Hsu, Appl. Phys. Lett. **95**, 223101 (2009).
16. O. Lupan, T. Pauporte, and B. Viana, Adv. Mater. **22**, 3298 (2010).
17. X. M. Zhang, M. Y. Lu, Y. Zhang, L. J. Chen, and Z. L. Wang, Adv. Mater. **21**, 2767 (2009).

Chapter Two

N-type Vertical ZnO Nanowire Array and Application in Dye-sensitized Solar Cell

2.1 Introduction

Potentially low-cost, flexible solar cells based on plastic substrates have attracted great interest for their super thin, lightweight and mechanically bendable characteristics [1-5]. They can be simply integrated on a curved structure, appropriate for wearable and portable applications. Recently, there is also an increased interest in developing solar cells based on nanowire arrays [6-15]. However, combining the large scale nanowire array and flexible substrate to make a dye-sensitized solar cell (DSSC) is challenging because typical flexible substrates cannot resist the process temperatures of up to 600 $^{\circ}$C generally used for the nanowire growth using chemical vapor deposition process [16, 17]. Even though some promising routes of low-temperature growth of nanowires [18, 19] on the plastic substrate have been reported, those nanowires cannot compete regarding electrical properties with nanowires obtained with the standard high-temperature process.

ZnO is semiconductor with a large wide band gap (3.3 eV) and very high electronic carrier mobility and electron affinity [20], making it a very possible candidate as an effective DSSC semiconductor. The great properties of vertically aligned ZnO-nanowire array, such as large surface area and fast electron-transport rate, make it a very promising option for the photoanode of DSSCs. Nanowires provide electrons injected from optically excited dye a direct effective path to collecting electrode via the semiconductor

conduction band, offering the potential for much faster charge transport than nanoparticle cells. On the other hand, unlike the bulk materials, nanowire array embedded in polymer film combines the benefits of flexibility and enhanced light absorption. Recently, a silicon wire array peel-off technique has been described in detail, which can yield a flexible nanowire-array for photovoltaic applications [21, 22]. However there is no such a report on transfer of ZnO nanowire array as well as its application on DSSC. In this chapter, we fabricated a flexible DSSC based on transferred vertically aligned ZnO nanowire array grown in CVD. The resulting device shows good photovoltaic effect and mechanical bendability. Furthermore, the large shunt resistance of DSSC, which comes from the great intactness of transferred nanowire array, results in a good fill factor (FF) of the solar cell.

2.2 Experimental Section

Highly oriented vertical ZnO nanowire array was successfully synthesized via seed growth method [23]. Firstly, ZnO seed-layer of about 100 nm was grown on sapphire substrate using a molecular beam epitaxy (MBE) system, Elemental zinc (6N) was evaporated with an effusion cell temperature of 360 $^{\circ}$C. The oxygen (5N) plasma was generated with a radio-frequency plasma source, while the growth temperature was kept at 550°C for 3 hours. The MBE-grown ZnO seed film was then cut and loaded into a conventional quartz CVD furnace for the growth of nanowire array, which was carried out at 600°C for 30 minutes with a zinc powder source inside and a mixture of argon (1000 sccm) and oxygen (1 sccm) flow.

After achieving the highly oriented vertical ZnO nanowire array, the peeling-off and transfer were performed by the process described below. The most crucial aspect for the successful transfer of large area vertical ZnO nanowire array onto the flexible substrate is how to form one non-fragile and elastic polymer film at the bottom of the nanowire array. Polydimethylsiloxane (PDMS) was used in the transfer process for its mechanically and chemically robust property. PDMS solution was made by completely mixing base and curing agent (10:1 w/w) of Sylgard 184. Then the uncured PDMS was diluted (5:1 w/w) by methylene-chloride-dissolved hexamethylcyclotrisiloxane, which would evaporate very fast upon heat, resulting in the polymer film achieving a desired thickness. The solution was then dropped onto the nanowire-array, which was followed by spinning at 2000 rpm for 1 min. As a result, one layer of transparent polymer film was formed on the bottom of ZnO nanowire array. Then one hour oven-heating at 150 $^{\circ}$C was carried out to cure and solidify the polymer. When the PDMS film became solid, a normal razor blade was used for the peeling-off, the nanowire-array can be mechanically removed from the sapphire substrate while pushing the blade between PDMS layer and sapphire substrate. The free-standing flexible ZnO-nanowire/PDMS film was then transferred onto the PET/ITO flexible substrate pasted with silver paste as an electrically-conductive adhesion layer.

After transferring the ZnO nanowire array onto PET/ITO flexible substrate, a conventional DSSC fabrication was taken. The details of the fabrication of DSSC solar cell are shown in Fig. 2.1. The assembly of ZnO-nanowire array and PET/ITO was immersed overnight in 3×10^{-4} M Ru $(dcbpy)_2(NCS)_2$(dcbpy: 2,2'-bipyridine-4,4'-

dicarboxylic acid (N3) dye. The sensitized film was rinsed with methanol, blown dry with nitrogen, and then sandwiched to a platinum–coated (2nm) PET/ITO counter electrode prepared by E-Beam Evaporator deposition system. A Parafilm tape was used as a spacer layer between the counter electrode and ITO/PET substrate. The internal space was filled with a liquid electrolyte (0.5 M lithium iodide, 0.05 M iodine, 0.5 M 4-tertbutylpyridine, 0.6 M 1-methyl-3-propylimidazolium iodide in 3-methoxypropionitrile) by capillary action. The sandwich-type DSSC with an active area of 1 cm^2 was immediately employed to measure the cell performance.

All field-emission scanning electron microscopy (FE-SEM) analysis was performed on a Leo SUPRA 55 operating at 15 kV. XRD data was obtained on a Philips X-ray diffractometer in θ-2θ geometry. Photoluminescence(PL) measurements were acquired with a continuous wave HeCd laser operating at 325 nm. The device photovoltaic characteristics were measured by Agilent 4155C under Oriel solar simulator illumination (AM1.5G, 100 mW/cm^2).

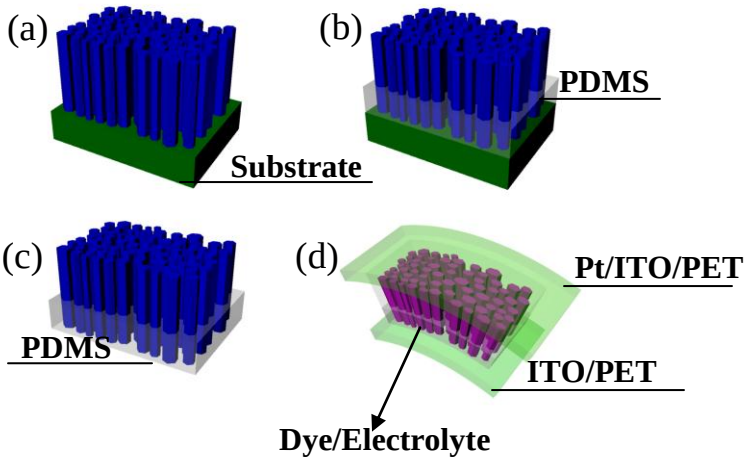

Figure 2.1 The process of flexible nanowire solar cell fabrication. (a) ZnO nanowires grown on hard substrate. (b) PDMS film casted into the nanowire array. (c) Peeled-off ZnO nanowire/PDMS film from the substrate. (d) Schematic view of the flexible solar cell containing a Pt (2nm)/ITO/PET top contact and an ITO/PET bottom contact. The ZnO nanowire was loaded with dye molecules.

2.3 Results and Discussion

XRD pattern in Fig.2. 2(a) suggests that the ZnO film grows preferentially along the c-direction of the ZnO wurtzite lattice. SEM images show the top view and side view of the ZnO seed film on sapphire substrate (Fig. 2.2(b) and (c)). The images indicate that vertical ZnO nano-columnar structures are formed, which is the typical result of oriented nucleation process arising from the large lattice mismatch between ZnO and sapphire substrate [24]. Fig. 2.2(d) is the SEM tilted view of the ZnO nanowire array on the ZnO seed layer, as can be seen, the ZnO nanowires nucleated on ZnO nano-columns and strictly maintained the c-axis orientation, resulting in a vertically aligned ZnO nanowire array. The length and diameter of the nanowire are averagely 15 μm and 200~400 nm, respectively.

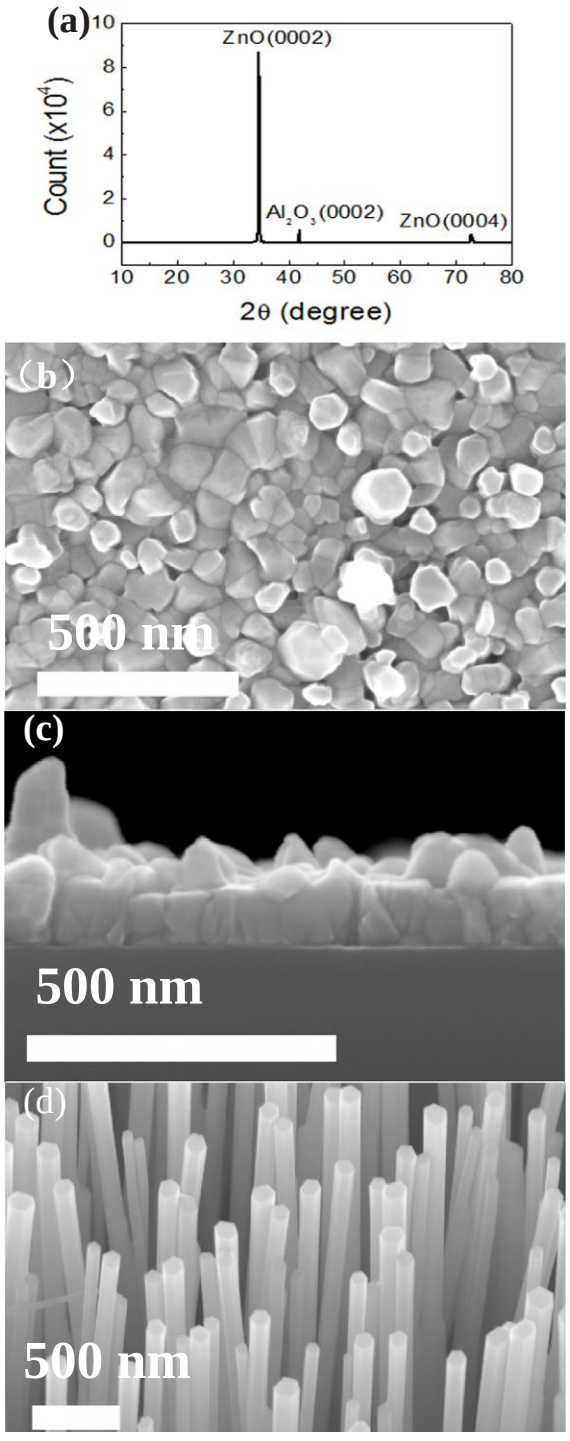
(a)
ZnO(0002)
Count (x10^4)
Al2O3(0002)
ZnO(0004)
2θ (degree)
(b)
500 nm
(c)
500 nm
(d)
500 nm

Figure 2.2 ZnO seed film and ZnO nanowire array growth. (a) XRD pattern of ZnO seed film; (b) Top view SEM image of the seed film;(c) Side view SEM image of the seed film, showing multiple nanocolumnar grains;(d) Tilted view SEM image of vertically aligned ZnO nanowire array grown on the seed film.

Fig. 2.3 shows the room-temperature optical property of ZnO nanowire array, which was examined by PL measurement. The strong peak at 374.7nm is the typical characteristic of ZnO near band edge emission, and the 500 nm band is normally attributed to oxygen vacancy [25].

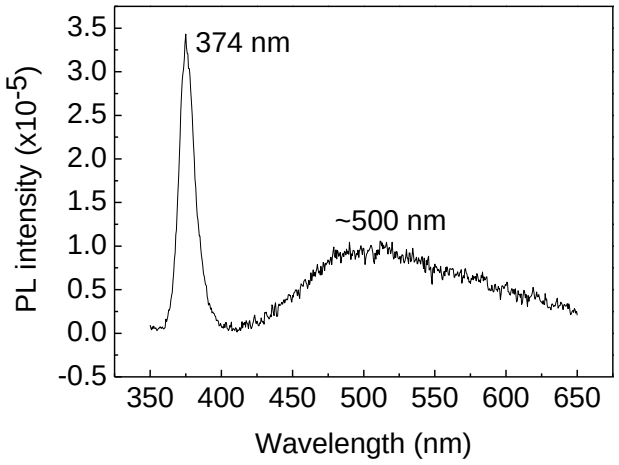

Figure 2.3 PL spectrum of ZnO nanowire array. The typical characteristic peak is observed at 374.7 nm and the 500 nm band is attributed to oxygen vacancy.

To examine the quality of peeled-off nanowire array embedded in PDMS films, SEM were again performed. Fig.2.4(a) is the image of peeled ZnO/PDMS layer on ITO/PET

substrate for further device application. As can be seen, it maintained very well alignment as compared to as grown samples. Fig. 2.4 (b) shows the ZnO/PDMS film while it was rolled up. It is very clear that the flexibility of the film is fairly good. The ZnO nanowire remains excellent directional alignment, which is a result of the balance of flexibility and hardness properties of PDMS.

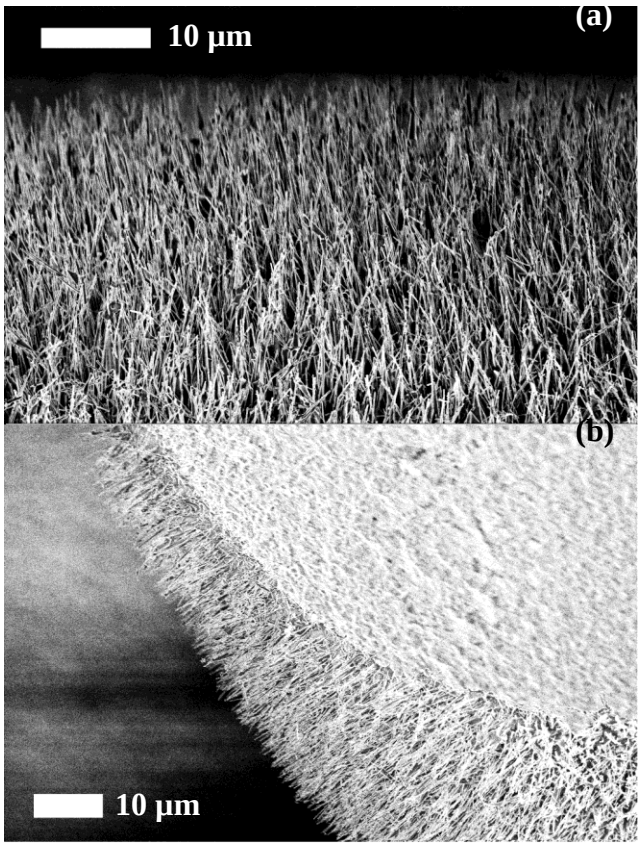

Figure 2.4 (a) The image of peeled ZnO/PDMS layer on ITO/PET substrate maintaining vertical alignment; (b) The rolled-up ZnO-nanowire/PDMS film.

The quality of the flexible nanowire DSSC device was evaluated by means of current density (J)–voltage (V) characteristics under illumination. In Fig. 2.5, such a J–V curve is

shown for illumination with simulated sunlight (air mass AM 1.5,100 mWcm^{-2}). Firstly, the solar cell was tested normally without bending. With a short circuit current J_{SC} = 0.75mAcm^{-2}, an open circuit voltage V_{OC} = 400 mV and a fill factor of 41%, the maximum power conversion efficiency is calculated to be η=0.1% by the formula $\eta = \frac{J_{SC} \times V_{OC} \times FF}{100W}$, (FF is fill factor), which is comparable to recently reported result [14]. The severely bent DSSC with the bending radius of approximately 5mm shows obvious degradation of efficiency from 0.1% to 0.069%, which might be a result of increasing leaking effect.

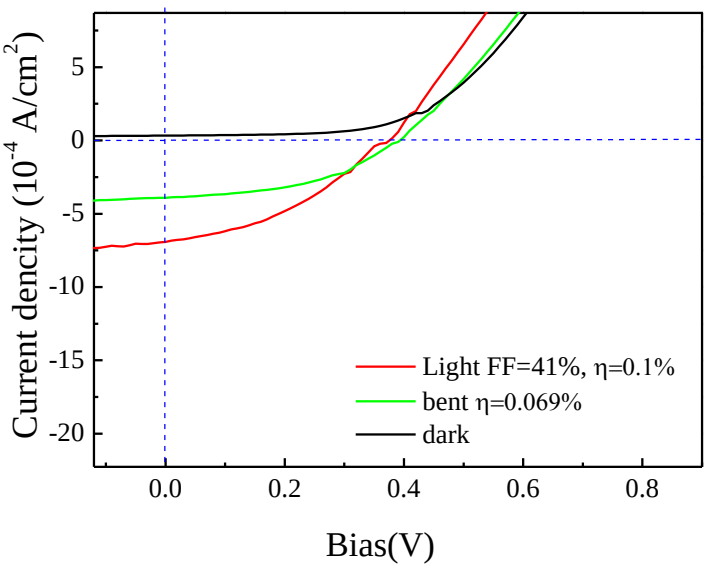

Figure 2.5 Current-Voltage curve of the nanowire array DSSC: black line: J-V curve under dark environment; red line: J-V curve under illumination; green line: J-V curve for bent DSSC under illumination. Bending radius: 5 mm.

The series resistance (R_s) and shunt resistance (R_{sh}) can be extracted by the slope of

the tangent line at Voc and the slope of the tangent line at Jsc respectively. The cell internal resistances including R_s and R_{sh} strongly affect the fill factor which is a phenomenological quantity. The analysis of the slopes of the steep part from light current curve results in $R_s=(dV/dI)_{I=0}$ approximately 270 Ωcm^2, which was mainly introduced by the contact between the ZnO nanowire array, adhesion layer (silver paste) and ITO. Therefore, much room for further optimization of this contact for higher efficiency solar cells exists. Considering $R_{sh}=(dV/dI)_{V=0}$ under illumination, the cell R_{sh} of 1260 Ωcm^2 is fairly large, which indicates great intactness of transferred nanowire array.

2.4 Conclusion

A simple way is demonstrated to make the flexible DSSC based on the transfer of a large scale array of highly oriented vertical ZnO nanowires. The large shunt resistance of the DSSC, which greatly benefit from the intactness of the transferred nanowire array, results in a good fill factor. The resulting DSSC on flexible substrate achieved a prominent photovoltaic effect even if the device was operated under severe bending condition, which is very promising for future flexible optoelectronics application.

2.5 References

[1] C. Lungenschmied, G. Dennler, H. Neugebauer, S. N. Sariciftci, M. Glatthaar, T. Meyer, A. Meyer, Sol. Energy. Mater. Sol .Cells. 91 (2007) 379.

[2] C. Longo, A. F. Nogueira, M. A. De-Paoli, J. Phys. Chem. B. 106 (2002) 5925.

[3] M. Al-Ibrahim, H. K. Roth, U. Zhokhavets, G. Gobsch, S. Sensfuss, Sol. Energy.

Mater. Sol. Cells. 85 (2005) 13.

[4] F. C. Krebs, M. Jørgensen, K. Norrman, O. Hagemann, J. Alstrup, T. D. Nielsen, J. Fyenbo, K. Larsen, J. Kristensen, Sol. Energy. Mater. Sol. Cells. 93 (2009) 422.

[5] F. Kessler, D. Rudmann, Sol. Energy. 77 (2004) 685.

[6] M. Adachi, Y. Murata, J. Takao, J. Jiu, M. Sakamoto, F. M. Wang, J. Am. Chem. Soc. 126 (2004)14943.

[7] J. B. Baxter, E. S. Aydil, Appl. Phys. Lett. 86 (2005) 053114.

[8] M. Law, L. E. Greene, J. C. Johnson, R. Saykally, P. D. Yang, Nat. Mater. 4 (2005) 455.

[9] J. B. Baxter, E. S. Aydil, Sol. Energy. Mater. Sol. Cells. 90 (2006) 607.

[10] M. Law, L. E. Greene, A. Radenovic, T. Kuykendall, J. Liphardt, P. D. Yang, J. Phys. Chem. B. 110 (2006) 22652.

[11] L. Hu, G. Chen, Nano Lett. 7 (2007) 3249.

[12] K. Q. Peng, X. Wang, T. S. Lee, Appl. Phys. Lett. 92 (2008) 163103.

[13] J. R. Maiolo, III, H. A. Atwater, N. S. Lewis, J. Phys. Chem. C. 112 (2008) 6194.

[14] S. Chu, D. D Li, P. C. Chang, J. G. Lu, Nanoscale Res Lett, 6 (2011) 38.

[15] B. D. Yuhas, P. D. Yang, J. Am. Chem. Soc. 131 (2009) 3756.

[16] A. I. Hochbaum, R. Fan, R. R. He, P. D. Yang, Nano Lett. 5 (2005) 457.

[17] G. D. Yuan, W. J. Zhang, J. S. Jie, X. Fan, J. A. Zapien, Y. H. Leung, L. B. Luo, P. F. Wang, C. S. Lee, S. T. Lee, Nano Lett. 8 (2008) 2591.

[18] C. H. Lu, L. M. Qi, J. H. Yang, L. Tang, D. Y. Zhang, J. M. Ma, Chem. Commun. (2006) 3551.

[19] Y. Sun, N. G. Ndifor-Angwafor, D. J. Riley, M. N. R. Ashfold, Chem. Phys. Lett. 431 (2006) 352.

[20] X. D. Bai, E. G. Wang, P. X. Gao, Z. L. Wang, Nano Lett. 3 (2003) 1147.

[21] K. E. Plass, M. A. Filler, J. M. Spurgeon, B. M. Kayes, S. Maldonado, B. Brunschwig, H. Atwater, N. S. Lewis, Adv. Mater. 21 (2009) 325.

[22] J. M. Spurgeon, K. E Plass, B. M. Kayes, B. S. Brunschwig, H. Atwater, N. S. Lewis, Appl. Phys. Lett. 93 (2008) 032112.

[23] L. E. Greene, M. Law, D. H. Tan, M. Montano, J. Goldberger, G. Somorjai, P. D. Yang, Nano. Lett. 5 (2005)1231.

[24] J. W. Shin, J. Y. Lee, Y. S. No, T. W. Kim, W. K. Choi, J. Appl. Phys.100 (2006) 013526.

[25] H. Y. Lu, S. Y. Chu, S. S. Tan, J. Cryst. Growth. 269 (2004) 385.

Chapter Three

Ag-doped p-type ZnO Nanowires and Sb-doped p-type ZnO Nanowire Array

3.1 Introduction

ZnO, a wide-band-gap semiconductor with large exciton binding energy of 60 meV at room temperature [1, 2], is a promising candidate for optoelectronic devices such as blue-light emitting diodes [3, 4], ultraviolet laser diodes [5, 6] and photodiodes [7, 8]. It is well known that one of the biggest challenges toward good ZnO-based optoelectronic devices is the difficulty of reliably fabricating p-type ZnO due to the self-compensating effect from native defects (for example, oxygen vacancy V_o and zinc interstitial Zn_i) and/or H incorporation [9]. There has already been a great deal of efforts on the fabrication of p-type ZnO films by doping group I (Na, Ag) [10, 11] and group V elements (N, P, As, Sb) [12-15] as p-type dopants. In contrast, there have been only a few reports on p-type ZnO nanowires (doped with N, P and Na) [16-18]. Recently, researchers are interested in developing optoelectronic devices based on ZnO nanowires such as biosensors, ultraviolet detectors, ultraviolet light emitting diodes and electrically driven nanowire lasers. The growth of p-type ZnO nanowires with good stability will be an essential step for the applications of nanowires in nanoelectronics and optoelectronics. Ag, a group Ib element, was predicted to be an acceptor in ZnO when incorporated into substitutional Zn sites [19]. Indeed, researchers experimentally demonstrated reliable fabrication of p-type ZnO thin films doped with Ag on sapphire substrate [11] with hole concentrations up to 6×10^{17} cm^{-3} and also demonstrated the possibility of achieving Ag-

doped p-type ZnO nanowires [20, 21]. However, the electrical and optical properties of single-crystalline Ag-doped ZnO nanowires have not been comprehensively studied yet. In this chapter, we report the synthesis and characterization of single-crystalline Ag-doped p-type ZnO nanowires. P-type ZnO nanowires were grown from a mixture of zinc powder and silver (I) oxide using chemical vapor deposition (CVD). The incorporation of Ag was confirmed by selected-area energy-dispersive x-ray spectroscopy (SAEDX) and photoluminescence (PL) studies. Single-nanowire field effect transistors were subsequently fabricated, which exhibited hole conduction channels, confirming the p-type conductivity of the Ag-doped ZnO nanowires. Also in this chapter, Sb-doped p-type ZnO nanowire array will be only briefly discussed, since in the next three chapters, Sb-doped p-type ZnO nanowire array-based optoelectronic devices will be comprehensively studied.

3.2 Experimental Section

The growth of nanowires was performed at 730 ºC for 15 minutes with a gas mixture, containing 600 sccm nitrogen and 300 sccm argon/oxygen (99.5: 0.5). The mixture source of zinc powder and silver (I) oxide (1:2 in mass) in a quartz boat was placed in the center of the quartz tube. The silicon substrate was closely attached to the quartz boat on the downstream side.

The incorporation of Ag was confirmed by selected-area energy-dispersive x-ray spectroscopy. The formation of acceptor states was demonstrated by temperature- and excitation power-dependent photoluminescence measurements. Characterization of field-

effect transistors using Ag-doped ZnO nanowires as channels showed p-type conductivity of the nanowires with a hole concentration of 4.9×10^{17} cm^{-3} and a carrier mobility of approximately 0.18 $cm^2 V^{-1} S^{-1}$.

3.3 Results and Discussion

Figures 3.1(a) and (b) show a scanning electron microscopy (SEM) image of the nanowires from the top and a regular transmission electron microscopy (TEM) image of an individual nanowire, respectively. The length and diameter of the ZnO nanowires are on average 5 μm and 250 nm, respectively. The single-crystalline nature of the ZnO nanowires is revealed by high-resolution TEM (HR-TEM) image (Figure 3.1(c)) and the selected area electron diffraction (SAED) pattern analysis (the top inset of Figure 3.1(c)). The lattice constant is determined to be 0.529 nm as shown in the bottom inset of Figure 3.1(c), which also indicates the [001] growth direction of the nanowire. Figure 3.1(d) presents the SAEDX spectrum of the individual nanowire shown in Figure 3.1(b), confirming the incorporation of Ag. The average atomic content of Ag was estimated to be ~ 0.1 atom %.

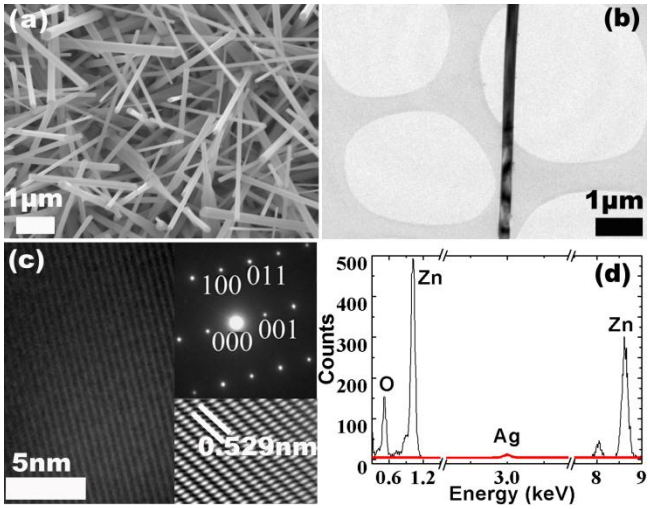

FIGURE 3. 1 (a) Top-view SEM image of as-grown ZnO nanowires. (b) TEM image of a single ZnO nanowire. (c) HR-TEM image of the nanowire. Inset images are (top) the SAED pattern and (bottom) a Fourier-filtered HR-TEM image. SAED pattern indicates the single-crystalline characteristic of the nanowire. The lattice spacing between two atomic layers is measured to be 0.529 nm. (d) SAEDX spectrum of the individual nanowire shown in (b).

To confirm the formation of acceptor levels by Ag doping, low-temperature PL measurements were performed with a 325 nm He–Cd laser operated at 89 μW. The laser beam impinged against the sample surface with an angle of approximately 60°. The excited PL emission was measured with an Oriel monochromator, which was aligned perpendicular to the sample surface. Figure 3.2(a) shows the temperature-dependent PL spectra of the Ag-doped sample at the temperatures ranging from 14 to 300 K. The emissions at 3.328 eV, 3.376 eV, 3.277 eV and 3.226 eV under the temperature of 14 K

can be assigned to be neutral-acceptor-bound exciton (A^oX), ground state of *A* free exciton ($FX_A^{n=1}$), free electron to acceptor level (FA) and donor-acceptor pair (DAP) transitions, respectively [22]. The appearance of different states of free excitons reflects the good optical property of the ZnO nanowires. The DAP emission at 3.226 eV shows a slightly progressive blueshift with an increase of temperature from 14 to 100 K, which is a result of thermal ionization of donors at higher temperatures and has been consistently reported as a typical characteristic of the DAP transition for ZnO [23, 24].

In Figure 3.2(b), the excitation power-dependent PL measurement results show the evolution of the DAP emission. The experiments were conducted at 14 K with different laser excitation power. With a decrease of the excitation power, the 3.226 eV emission exhibits an evident redshift. The peak energy of such transition is given by the following equation [12]:

$$E_{DAP} = E_{gap} - E_D - E_A + e^2 /4\pi\varepsilon R_{DAP} \quad (1)$$

where E_{DAP}, E_{gap}, E_D, E_A, e, ε and R_{DAP} are DAP transition energy, band gap energy, donor ionization energy, acceptor ionization energy, elementary charge constant, dielectric constant, and donor-acceptor pair distance, respectively. As the excitation intensity (power/area) decreases, the number of photo excited donor-acceptor pairs decreases, resulting in a longer donor-acceptor pair distance (R_{DAP}). Therefore, a DAP transition shifts to a lower energy.

Based on the FA peak position in Figure 3.2(a), the acceptor binding energy (E_A) at 14 K can be calculated with the equation [25]:

$$E_A = E_{gap} - E_{FA} + k_BT/2 \quad (2)$$

where E_{FA} is the temperature-dependent transition with an energy of 3.277 eV at 14 K, E_{gap} is the intrinsic band gap energy, which is approximately equal to 3.437 eV at 14 K, and k_B is Boltzmann constant. Thus, the value of E_A is calculated to be 0.158 eV.

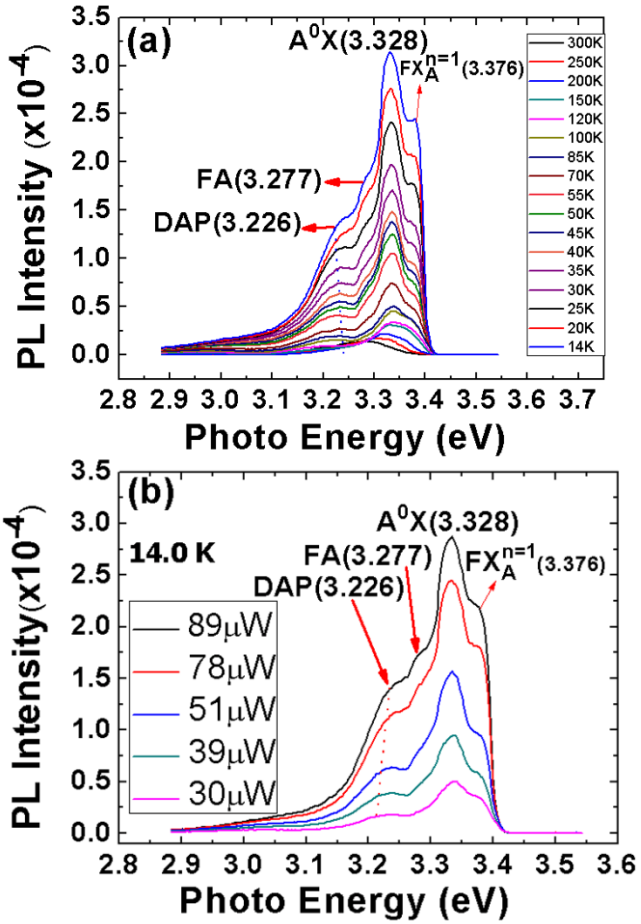

FIGURE 3.2 Low-temperature PL spectra of (a) Ag-doped ZnO nanowires at temperatures ranging from 14 to 300 K. (b) Ag-doped ZnO nanowires under different excitation power at 14 K.

In order to further prove p-type conductivity of the Ag-doped ZnO nanowires, electrical measurements on back-gated nanowire field effect transistors (NWFETs) were

carried out. ZnO NWFETs were fabricated by standard photolithography. Ag-doped ZnO nanowires were first dispersed in isopropyl alcohol and subsequently transferred to a p+- silicon wafer with a 300 nm thick silicon oxide on the surface. Micro-contact windows were defined on the ends of the nanowires, and then the Ni/Au electrodes were formed by e-beam deposition and subsequent lift-off. The p+- silicon substrate served as the back-gate electrode of the transistor. The inset in Figure 3.3(a) shows the SEM image of the NWFET. The drain current (I_d) versus gate voltage (V_g) curve under a drain bias (V_d) of 10 V and I_d versus V_d curves under different gate voltages are shown in Figure 3.3(a) and Figure 3.3(b), respectively.

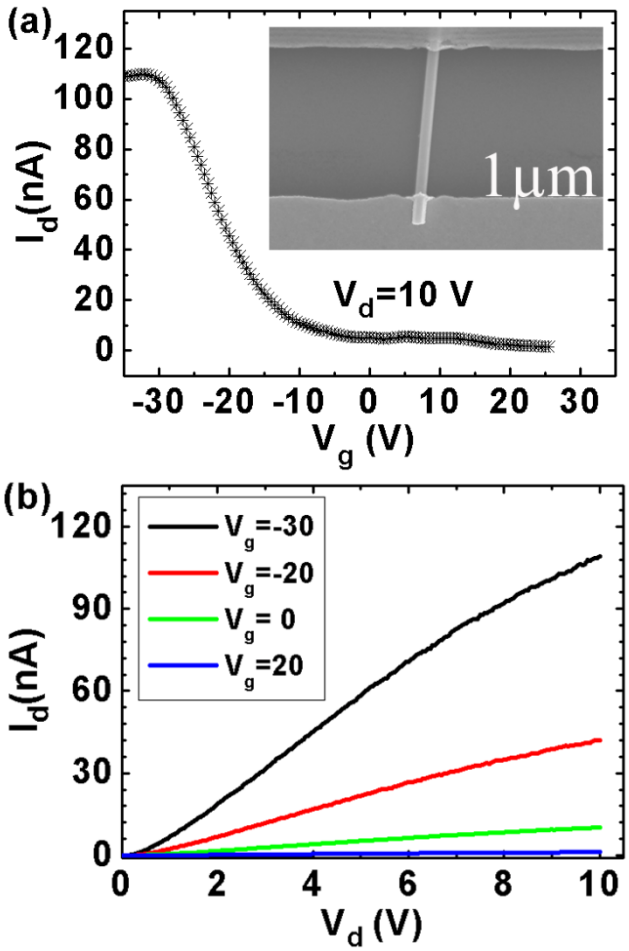

FIGURE 3.3 (a) I_d-V_g curve of the ZnO NWFET under V_d=10 V. Inset shows the SEM image of the NWFET. (b) I_d-V_d curves of the ZnO NWFET recorded at different gate voltages.

The drain current decreases as the increase of the gate voltage from -30 V to 30 V, suggesting that the Ag-doped ZnO nanowires exhibit *p*-type behavior. The hole concentration (P) in nanowires can be estimated by using the following equation [26]:

$$P = \left(\frac{V_{th}}{q}\right) \times \left(\frac{2\pi\varepsilon_r\varepsilon_o}{\ln(4h/d)}\right) \times \left(\frac{1}{\pi d^2/4}\right) \quad (3)$$

where ε_r, ε_0, h, d, V_{th}, and q are the effective dielectric constant (ε_r=3.9 for SiO_2), dielectric constant of vacuum, thickness of dielectric layer (300 nm), nanowire diameter (250 nm), threshold voltage of the ZnO NWFET (~28 V) and elementary charge constant, respectively. From eq.(3), the hole concentration is calculated to be 4.9×10^{17} cm^{-3}. The mobility can be calculated by using the equation [26]:

$$\mu = \left(\frac{dI}{dV_g}\right) \times \left(\frac{\ln\left(\frac{4h}{d}\right)}{2\pi\varepsilon_r\varepsilon_o}\right) \times \left(\frac{L}{V_d}\right) \qquad (4)$$

where μ, L and V_d is the mobility, channel length (~3μm in the NWFET) and drain bias (10 V), respectively. $\frac{dI}{dV_g}$ = 7.16e-009 A/V can be extrapolated from the linear region of the I_d-V_g curve. From eq.(4), the hole mobility is calculated as approximately 0.18 $cm^2V^{-1}s^{-1}$.

Top-view of SEM image of Sb-doped p-type ZnO nanowire array and the low temperature PL spectra are shown in Figure 3.4(a) and 3.4(b), respectively. In Figure 3.4(b), Sb-doped ZnO nanowires spectrum shows distinct neutral-acceptor-bound exciton (A^0X) peak at 3.350 eV. In addition, this peak becomes significantly wider than D^0X in the undoped ZnO nanowire, which is due to extensive dopant incorporation. More evidences of *p*-type behavior of the nanowires are shown in the next three chapters when discussing the application of these nanowire arrays into optoelectronic devices.

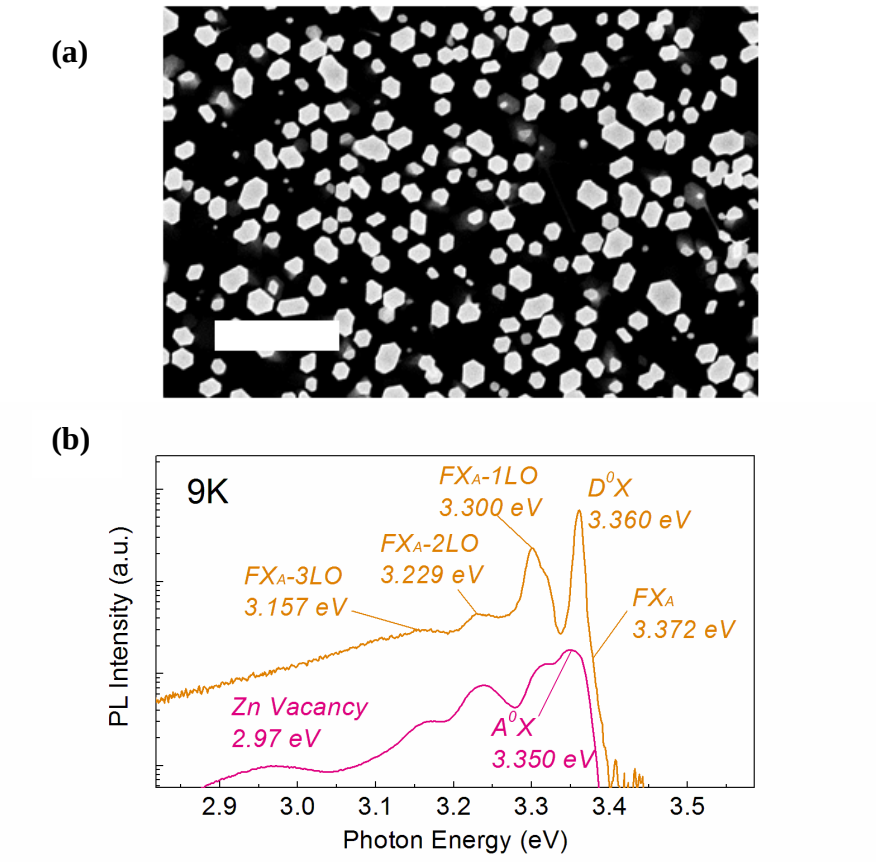

Figure 3.4 (a) Top-view SEM image of as grown Sb-doped nanowire array. Scale bar: 1 μm. (b) PL spectra of undoped ZnO nanowires (top curve) and Sb-doped ZnO nanowires (bottom curve).

3.4 Conclusion

Ag-doped ZnO nanowires have been grown via CVD process. The PL spectrum of the Ag-doped nanowires shows an Ag-related peak at 3.328 eV at 14 K, which can be attributed to neutral-acceptor-bound excitons (A^0X). Temperature- and excitation power-dependent PL spectra confirm shallow acceptor level of 0.158 eV. The electrical

measurement results suggest that the conductivity of Ag-doped ZnO nanowires is *p*-type and the hole mobility is approximately 0.18 $cm^2 V^{-1} S^{-1}$. After 5 months, however, originally p-type Ag-doped ZnO nanowires turned into n-type judging from NWFET measurements. Therefore, long-term p-type stability of Ag-doped ZnO nanowires is still an issue. P-type Sb-doped ZnO nanowire array was also achieved. The shallow-acceptor induced energy level of the Sb-doped ZnO nanowire array was observed by low-temperature PL at 3.350 eV.

3.5 References

1. E. O. Kane, Phys. Rev. B **18**, 6849 (1978).
2. C. Klingshirn, Phys. Status. Solidi. B **244**, 3027(2007).
3. D. C. Look, Mater. Sci. Eng., B **80**, 383 (2001).
4. S. Chu, J. H. Lim, L. J. Mandalapu, Z. Yang, L. Li, J. L. Liu, Appl. Phys. Lett. **92**,152103 (2008).
5. S. F. Yu, C. Yuan, S. P. Lau, W. I. Park, G. Yi, Appl. Phys. Lett. **84**, 3241 (2004).
6. L. K. van Vugt, S. Ruhle, D. Vanmaekelbergh, Nano Lett. **6**, 2707 (2006).
7. L. J. Mandalapu, F. X. Xiu, Z. Yang, D. T. Zhao, J. L. Liu, Appl. Phys. Lett. **88**, 112108 (2006).
8. L. J. Mandalapu, Z. Yang, F. X. Xiu, D. T. Zhao, J. L. Liu, Appl. Phys. Lett. **88**, 092103 (2006).
9. C. G. Van de Walle, Phys. Rev. Lett. **85**, 1012 (2000).
10. S. S. Lin, H. P. He, Y. F. Lu, Z. Z. Ye, J. Appl. Phys. **106**, 093508 (2009).

11. H. S. Kang, B. D. Ahn, J. H. Kim, G. H. Kim, S. H. Lim, H. W. Chang, S. Y. Lee, Appl. Phys. Lett. **88**, 202108 (2006).

12. D. K. Hwang, H. S. Kim, J. H. Lim, J. Y. Oh, J. H. Yang, S. J. Park, K. K. Kim, D. C. Look, Y. S. Park, Appl. Phys. Lett. **86**, 151917 (2005).

13. K. K. Kim, H. S. Kim, D. K. Hwang, J. H. Lim, S. J. Park, Appl. Phys. Lett. **83**, 63 (2003).

14. T. S. Jeong, M. S. Han, C. J. Youn, Y. S. Park, J. Appl. Phys. **96**, 175 (2004).

15. F. X. Xiu, Z. Yang, L. J. Mandalapu, D. T. Zhao, J. L. Liu, W. P. Beyermann, Appl. Phys. Lett. **87**, 152101(2005).

16. B. Xiang, P. W. Wang, X. Z. Zhang, S. A. Dayeh, D. P. Aplin, C. Soci, D. P. Yu, D. L. Wang, Nano Lett. **7**, 323 (2007).

17. G. D. Yuan, W. J. Zhang, J. S. Jie, X. Fan, J. A. Zapien, Y. H. Leung, L. B. Luo, P. F. Wang, C. S. Lee, S. T. Lee, Nano Lett. **8**, 2591 (2008).

18. W. Liu, F. X. Xiu, K. Sun, Y. H. Xie, K. L. Wang, Y. Wang, J. Zou, Z. Yang, J. L. Liu, J. Am. Chem. Soc. **132**, 2498 (2010).

19. Y. Kanai, Jpn. J. Appl. Phys., Part 1 **30**, 2021 (1991).

20. Y. W. Song, K. Kim, J. P. Ahn, G. E. Jang, S. Y. Lee, Nanotechnology **20**, 275606, (2009).

21. M. A. Thomas, J. B. Cui, J. Phys. Chem. Lett. **1**, 1090 (2010).

22. Ü. Özgür. Ya, I. Alivov, C. Liu, A. Teke, M. A. Reshchikov, S. Doğan, V. Avrutin, S.-J. Cho, H. Morkoç, J. Appl. Phys. **98**, 041301 (2005).

23. K. Tamura, T. Makino, A. Tsukazaki, M. Sumiya, S. Fuke, T. Furumochi, M.

Lippmaa, C. H. Chia, Y. Segawa, H. Koinuma, M. Kawasaki, Solid State Commun. **127**, 265(2003).

24. K. Thonke, T. Gruber, N. Teofilov, R. Schonfelder, A. Waag, R. Sauer, Physica B **308**, 945 (2001).
25. Y. R. Ryu, T. S. Lee, H. W. White, Appl. Phys. Lett. **83**, 87 (2003).
26. R. Martel, T. Schmidt, H. R. Shea, T. Hertel, Ph. Avouris, Appl. Phys. Lett. **73**, 2447, (1998).

Chapter Four

ZnO Homojunction Photodiodes based on Sb-doped p-type Nanowire Array and n-type Film for Ultraviolet Detection

4.1 Introduction

ZnO has a wide band gap of 3.37 eV and a large exciton binding energy of 60 meV at room temperature,[1,2] which make it a promising candidate for optoelectronic devices such as blue-light emitting diodes,[3,4] ultraviolet laser diodes[5-7] and photodiodes.[8-10] Recently, there have been tremendous interests in ZnO nanowire arrays. Although heterojunction optoelectronic devices[11-13] have been fabricated based on vertically aligned ZnO nanowire arrays, there still lacks the homojunction type devices based on p-type nanowire array/n-type ZnO film. It is well known that one of the biggest challenges toward good ZnO-based optoelectronic devices is the difficulty of reliably fabricating p-type ZnO due to the self-compensating effect from native defects (for example, oxygen vacancy V_o and zinc interstitial Zn_i) and/or H incorporation.[14] Nevertheless, there has already been a great deal of efforts on the fabrication of p-type ZnO by doping group V elements, such as N, P, As.[15-17]Previously, our group showed that Sb, another group V element, is an effective dopant for reproducible p-type ZnO thin films[18] on Si and sapphire substrates. Heterojunction[8] and homojunction[9] light emitting diodes as well as photodiodes based on these films were achieved. In this study, we report ZnO p-n homojunctions based on Sb-doped p-type ZnO nanowire arrays grown by chemical vapor deposition (CVD) on n-type ZnO films on sapphire substrates grown by molecular-beam epitaxy (MBE). The homojunction diode exhibits a clear rectification characteristic as

well as very good ultraviolet light absorption characteristics.

4.2 Experimental Section

The device fabrication process of the p-type ZnO nanowire/n-type ZnO film structure is described as follows. Highly oriented vertical ZnO nanowire array was synthesized via seed growth method.[19] First, n-type ZnO seed film, which also acted as n-type component of the junction, was grown on a 2-inch c-plane sapphire substrate using plasma-assisted MBE. The growth process began with a thin MgO/ZnO buffer layer of less than 10 nm at a growth temperature of 550 ºC for improving the subsequent ZnO film quality. Then the seed ZnO film was grown at 700 ºC for 5 hours, yielding a total thickness of around 1050 nm. Elemental Zn was evaporated at an effusion cell temperature of 360 ˚C. The oxygen plasma was generated using a radio-frequency plasma source. The oxygen flow rate was kept at 5 sccm. Hall effect measurements were carried out on the MBE-grown ZnO thin film. The film was found to have n-type conductivity with an electron concentration of $3.74\times10^{17}cm^{-3}$, mobility of 23.04 $cm^2\ V^{-1}S^{-1}$ and resistivity of 0.73 Ωcm, respectively. The ZnO seed film was partially covered for exposing the film for later n-type contacts deposition and then subsequently transferred into a quartz tube furnace system. The growth of nanowire array was carried out at 650ºC for 15 minutes with a gas flow of 1000 sccm nitrogen and 200 sccm mixture gas of argon/oxygen (99.5: 0.5). Zn powder source (99.999%) in a glass bottle was placed in the center of the quartz tube. At the place of ~5 cm upstream to the Zn powder source, Sb powder (99.99%) was placed in an open glass boat. The ZnO seed film was kept around

10 cm away from the Zn source on the down-stream side. After vertical nanowire array was achieved in CVD, polymethyl-methacrylate (PMMA) was spun on the sample to separate the bottom ZnO film and the subsequent top ITO contact layer. The spin speed was 2000 rpm for 30 seconds and this process was repeated for 5 times. After the sample was dried, a thin layer of ITO was sputtered by a sputter evaporator on the top of ZnO nanowire array. The sputtering process was performed at room temperature and the pressure was maintained at 10^{-2} Torr. The sputtering power and time were 180 watt and 10 minutes, respectively. After the growth of ITO, acetone was used to remove PMMA layer. The device was finished by depositing Ti/Au (20nm/100nm) on the n-type ZnO film using an e-beam evaporator and rapidly annealed under 600ºC for 1 minute to improve conductivity. Another low-resistant ITO glass slide was placed on the top of the ZnO nanowire array when I-V and photoresponse characteristics were measured. Figure 4.1 shows schematic diagram of the device.

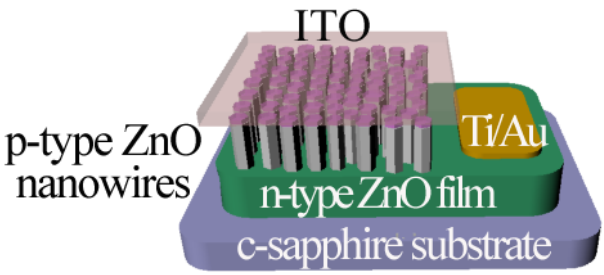

FIGURE 4. 1 Schematic view of the photodetector device, which consists of ZnO thin film on c-sapphire substrate, vertically aligned ZnO nanowires, ITO contacts and Ti/Au contacts.

4.3 Results and Discussion

Figures 4.2(a) and (b) show scanning electron microscopy (SEM) images of the nanowire array from the top and the side, respectively. Typical wurtzite hexagonal structure ZnO nanowires are evident. The length and diameter of the ZnO nanowires are on average 3 μm and 150 nm, respectively. The single crystalline nature of the ZnO nanowires is confirmed by high-resolution transmission electron microscopy (TEM) analysis, as shown in Figure 4.2(c) and by the selected area electron diffraction (SAED) pattern (Figure 4.2(d)).

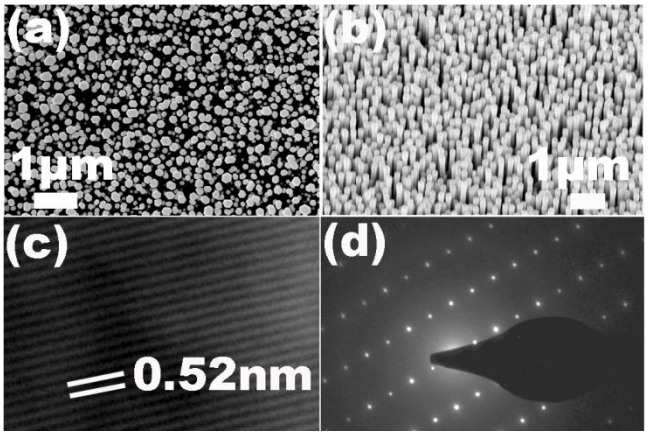

FIGURE 4.2 (a) Top-view and (b) side-view SEM images of as-grown p-type ZnO nanowires. (c) High-resolution TEM image of a single nanowire. The lattice spacing between two atomic layers is measured to be 0.52 nm. (d) SAED pattern, indicating the single-crystalline characteristic of the nanowire.

Figure 4.3(a) shows spectrum of the electron beam induced current (EBIC) profiling of the homojunction between the ZnO nanowires and ZnO film superimposed on the

side-view SEM image of the device. As a versatile tool, EBIC was widely used to identify buried junctions in semiconductors, including characterization of ZnO thin film p-n junctions[20] and silicon nanowire p-n junctions.[21]In the experiment, electron-hole pairs are generated by electron beam irradiation. Then they are separated by built-in electric field in the p-n junction depletion region and collected by external amplifier. Here, accelerating voltage of 30 kV was applied, corresponding to electron penetration depth of 1.5 μm. Silver paste instead of ITO glass was used as contact to the p-type nanowires for facilitating the EBIC experiment. As seen from Figure 4.3(a), EBIC signal forms a peak on the thin film/nanowire junction, indicating the formation of p-n junction. Second peak on the right is due to the formation of the nanowire/ITO/silver paste semiconductor-metal junction.

P-type conductivity of the Sb-doped ZnO nanowires can also be proved by field-effect measurement. ZnO nanowire field effect transistors (NWFETs) were fabricated by standard photolithography. Sb-doped ZnO nanowires were transferred to a p+-silicon wafer with a 300 nm thick silicon oxide on the surface. Micro-contact windows were defined on the ends of the nanowires, then Ni/Au (20 nm/100 nm) electrodes were formed by e-beam deposition and subsequent lift-off. The p+-silicon substrate served as the back-gate electrode of the transistor. The inset in Figure 4.3(b) shows a SEM image of the NWFET. The drain current (I_d) vs gate voltage (V_g) curve under a drain voltage (V_d) of 10 V and I_d vs V_d curves under different gate voltages are shown in Figure 4.3(b) and Figure 4.3(c), respectively. The results show that the Sb-doped ZnO nanowires exhibit p-type behavior under gate voltage ranging from -10 V to 30 V. The origin of the p-type

conductivity of the Sb-doped ZnO nanowires is from the shallow acceptors formed by substitutional Sb_{Zn} simultaneously connecting two Zn vacancies.[22] The hole concentration (P) in nanowires can be estimated by using the following equation:[23]

$$P = \left(\frac{V_{th}}{q}\right) \times \left(\frac{2\pi \varepsilon_r \varepsilon_o}{\ln(4h/d)}\right) \times \left(\frac{1}{\pi d^2/4}\right) \quad (1)$$

where ε_r, ε_o, h, d, $V_{th,}$ and q are the effective dielectric constant (3.9 for SiO_2), dielectric constant in vacuum, the thickness of dielectric layer (300 nm), nanowire diameter (~200 nm), the threshold voltage of the ZnO NWFET (~29 V) and elementary charge constant, respectively. From eq.(1), the hole concentration is calculated to be 6.9×10^{17} cm^{-3}. The mobility can be calculated by using the equation:[23]

$$\mu = \left(\frac{dI}{dV_g}\right) \times \left(\frac{\ln\left(\frac{4h}{d}\right)}{2\pi \varepsilon_r \varepsilon_o}\right) \times \left(\frac{L}{V_d}\right) \quad (2)$$

where μ, L and V_d is the mobility, channel length (~1.8 μm) and drain-source voltage (10 V), respectively. $\frac{dI}{dV_g}$ = 2.55e-009 A/V can be extrapolated from the linear region of the I_d-V_g curve. From eq.(2), the mobility is calculated as approximately 0.037 cm^2V^{-1} s^{-1} based on the experimental data.

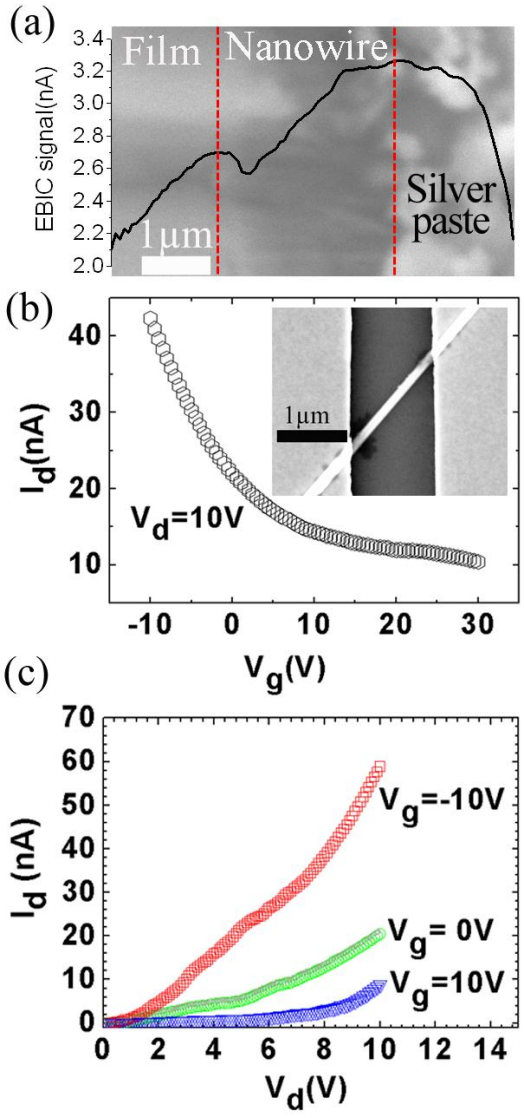

FIGURE 4.3 (a) EBIC profile of the device. A clear peak can be seen in the area between the ZnO nanowires and ZnO film, representing the formation of junction. (b) I_d-V_g curve of the ZnO nanowire FET under V_d=10 V. Inset shows the SEM image of the NWFET. (c) I_d-V_d curves of the ZnO nanowire FET recorded at different gate voltages.

Figure 4.4(a) shows current-voltage characteristics of the ZnO p-n homojunction. Clear rectifying behavior can be observed with and without ultraviolet (UV) illumination. The turn-on voltage is ~3V. Photocurrent (PC) measurements were carried out using a home-built system. The PC system consists of an Oriel Xe arc lamp as the UV source. The light from the lamp passes through an Oriel 0.25 m monochromator, which produces a specific wavelength light at its output port. After chopping, the light is then cast on the device. The generated PC signal is fed to a lock-in amplifier from where the data is collected. Figure 4.4(b) shows PC spectra of the homojunction device operated in the photovoltaic mode and also under different reverse biases. The device shows response as a result of the photocarriers generated by the absorption of light in the space-charge region. The response extends from 280 nm and steadily increases up to 380 nm (3.26 eV), which corresponds to the effective band gap of ZnO. The magnitude of photocurrent increases with the increase of applied reverse bias (-2V,-4V, -6V) due to enhanced carrier collection. There is a small peak at 570 nm (2.17 eV) in the spectra due to the presence of deep levels in ZnO.

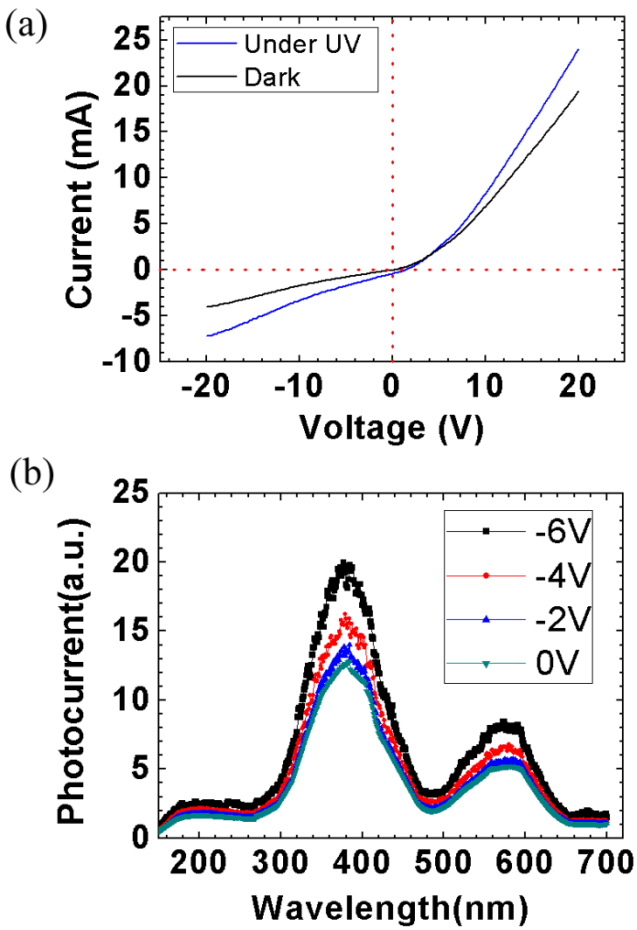

FIGURE 4.4 (a) I-V characteristics of the ZnO nanowire/ZnO film device with and without UV illumination. (b) PC spectra under different reverse biases. Good responses in the UV region are evident.

4.4 Conclusion

ZnO p-n homojunctions based on Sb-doped p-type nanowire arrays and n-type thin films were grown by the combination of CVD and MBE. The ZnO thin film/nanowire p-n junction was proved by EBIC profiling, I-V measurement, and field-effect measurement. Evident photoresponse was observed in the UV region of the PC spectra. This study not only proved that Sb doping can lead to p-type ZnO nanowires but also demonstrated an ultraviolet homojunction photodetector device based on p-type nanowire array and n-type thin film.

4.5 References

[1] E. O. Kane, Phys. Rev. B **18**, 6849 (1978).

[2] C. Klingshirn,Phys. Status. Solidi. B **244**, 3027(2007).

[3] D. C. Look, Mater. Sci. Eng. B **80**, 383 (2001).

[4] S. Chu, J. H. Lim, L. J. Mandalapu, Z. Yang, L. Li, and J. L. Liu, Appl. Phys. Lett. **92**, 152103 (2008).

[5] H. Cao, Y. G. Zhao, H. C. Ong, S. T. Ho, J. Y. Dai, J. Y. Wu, and R. P. Chang, Appl. Phys. Lett. **73**, 3656 (1998).

[6] S. F. Yu, C. Yuan, S. P. Lau, W. I. Park, and G. Yi, Appl. Phys. Lett. **84**, 3241 (2004).

[7] S. Chu, M. Olmedo, Z. Yang, J. Y. Kong, and J. L. Liu, Appl. Phys. Lett. **93**, 181106 (2008).

[8] L. J. Mandalapu, F. X. Xiu, Z. Yang, D. T. Zhao, and J. L. Liu, Appl. Phys. Lett. **88**, 112108 (2006).

[9] L. J. Mandalapu, Z. Yang, F. X. Xiu, D. T. Zhao, and J. L. Liu, Appl. Phys. Lett. **88**,

092103 (2006).

[10]L. J. Mandalapu, F. X. Xiu, Z. Yang, and J. L. Liu, Solid State Electronics **51**, 1014 (2007).

[11] C. H. Chen, S. J. Chang, S. P. Chang, M. J. Li, I. C. Chen, T. J. Hsueh, and C. L. Hsu, Appl. Phys. Lett. **95**, 223101 (2009).

[12] O. Lupan, T. Pauporte, and B. Viana, Adv. Mater. **22**, 3298 (2010).

[13] X. M. Zhang, M. Y. Lu, Y. Zhang, L. J. Chen, and Z. L. Wang, Adv. Mater. **21**, 2767 (2009).

[14] C. G. Van de Walle, Phys. Rev. Lett. **85**, 1012 (2000).

[15] D. K. Hwang, H. S. Kim, J. H. Lim, J. Y. Oh, J. H. Yang, S. J. Park, K. K. Kim, D. C. Look, and Y. S. Park, Appl. Phys. Lett. **86**, 151917 (2005).

[16] K. K. Kim, H. S. Kim, D. K. Hwang, J. H. Lim, and S. J. Park, Appl. Phys. Lett. **83**, 63 (2003).

[17] T. S. Jeong, M. S. Han, C. J. Youn, and Y. S. Park, J. Appl. Phys. **96**, 175 (2004).

[18] F. X. Xiu, Z. Yang, L. J. Mandalapu, D. T. Zhao, and J. L. Liu, Appl. Phys. Lett. **87**, 152101 (2005).

[19] L. E. Greene, M. Law, D. H. Tan, M. Montano, J. Goldberger, G. Somorjai, and P. D. Yang, Nano. Lett. **5**, 1231 (2005).

[20] L. Chernyak, C. Schwarz, E. S. Flitsiyan, S. Chu, J. L. Liu, and K. Gartsman, Appl. Phys. Lett. **92**, 102106 (2008)

[21] S. Hoffmann, J. Bauer, C. Ronning, Th. Stelzner, J. Michler, C. Ballif, V. Sivakov, and S. H. Christiansen, Nano. Lett. **9**, 1341 (2009).

[22] S. Limpijumnong, S. B. Zhang, S. H. Wei, and C. H. Park, Phys. Rev. Lett. **92**, 155504 (2004).

[23] R. Martel, T. Schmidt, H. R. Shea, T. Hertel, and Ph. Avouris, Appl. Phys. Lett. **73**, 2447, (1998).

Chapter Five

ZnO Homojunction LEDs based on Sb-doped p-type Nanowire Array and n-type Film

5.1 Introduction

ZnO, a semiconductor with a wide band gap of 3.37 eV and a large exciton binding energy of 60 meV at room temperature[1,2], recently has been extensively studied for ultraviolet (UV)/blue optoelectronic applications such as light emitting diodes (LEDs) [3,4] and laser diodes.[5–7] It is well known that it is extremely difficult to achieve reliable p-type ZnO due to the self-compensating effect from native defects induced during material growth, which can act as shallow donors (for example, oxygen vacancy V_o and zinc interstitial Zn_i) and/or H incorporation.[8] Nevertheless, many research groups have reported the fabrication of *p*-type ZnO and ZnO LEDs by doping group V elements, such as N, P, As.[9-11] Previously, Sb, another group V element, was shown to be an effective dopant for reproducible p-type ZnO thin films[12] on Si and sapphire substrates. Heterojunction[13] and homojunction[14] light emitting diodes as well as photodiodes based on these films were achieved. However, no LEDs based on ZnO nanowires were reported. Recently, there have been tremendous interests in ZnO nanowire arrays. Although heterojunction optoelectronic devices[15-16] have been fabricated based on vertically aligned ZnO nanowire arrays, there is lack of homojunction type devices based on p-type nanowire array/n-type ZnO film. In this study, we report ZnO p-n homojunctions based on Sb-doped p-type ZnO nanowire arrays grown by chemical vapor deposition (CVD) on n-type ZnO films on sapphire substrates grown by molecular-beam epitaxy (MBE). The

homojunction diode exhibits a clear rectification characteristic as well as very good near-band-edge (NBE) emissions at room temperature.

5.2 Experimental Section

The device fabrication process of the p-type ZnO nanowire/n-type ZnO film structure is described as follows. Highly oriented vertical ZnO nanowire array was synthesized via seed growth method.[17] First, n-type ZnO seed film, which also acted as n-type component of the junction, was grown on a 2-inch c-plane sapphire substrate using plasma-assisted MBE. The growth process began with a thin MgO/ZnO buffer layer of less than 10 nm at a growth temperature of 550 ºC for improving the subsequent ZnO film quality. Then the seed ZnO film was grown at 700 ºC for 5 hours, yielding a total thickness of around 1050 nm. Elemental Zn was evaporated at an effusion cell temperature of 360 ˚C. The oxygen plasma was generated using a radio-frequency plasma source. The oxygen flow rate was kept at 5 sccm. Hall effect measurements were carried out on the MBE-grown ZnO thin film. The film was found to have n-type conductivity with an electron concentration of $3.74\times10^{17}cm^{-3}$, mobility of 23.04 $cm^2\ V^{-1}S^{-1}$ and resistivity of 0.73 Ωcm, respectively. The ZnO seed film was partially covered for exposing the film for later n-type contacts deposition and then subsequently transferred into a quartz tube furnace system. The growth of nanowire array was carried out at 650ºC for 15 minutes with a gas flow of 1000 sccm nitrogen and 200 sccm mixture gas of argon/oxygen (99.5: 0.5). Zn powder source (99.999%) in a glass bottle was placed in the center of the quartz tube. At the place of ~5 cm upstream to the Zn powder source, Sb

powder (99.99%) was placed in an open glass boat. The ZnO seed film was kept around 10 cm away from the Zn source on the down-stream side. After vertical nanowire array was achieved in CVD, polymethyl-methacrylate (PMMA) was spun on the sample to separate the bottom ZnO film and the subsequent top ITO contact layer. The spin speed was 2000 rpm for 30 seconds and this process was repeated for 5 times. After the sample was dried, a thin layer of ITO was sputtered by a sputter evaporator on the top of ZnO nanowire array. The sputtering process was performed at room temperature and the pressure was maintained at 10^{-2} Torr. The sputtering power and time were 180 watt and 10 minutes, respectively. After the growth of ITO, acetone was used to remove PMMA layer. The device was finished by depositing Ti/Au (20nm/100nm) on the n-type ZnO film using an e-beam evaporator and rapidly annealed under 600ºC for 1 minute to improve conductivity. Another low-resistant ITO glass slide was placed on the top of the ZnO nanowire array when I-V and photoresponse characteristics were measured. Figure 5. 1 shows schematic diagram of the device.

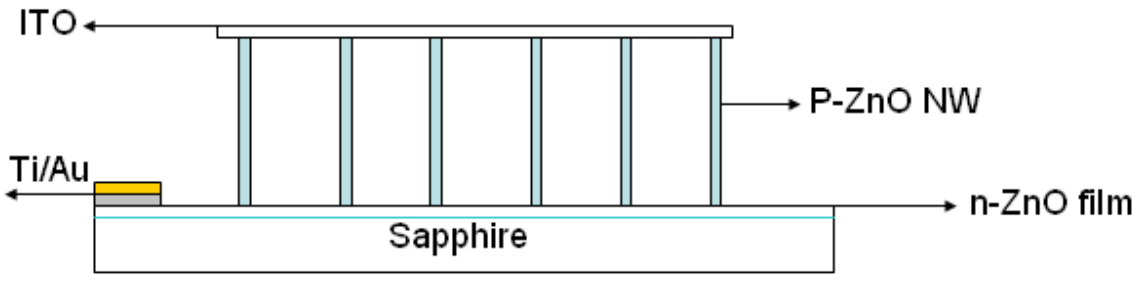

FIGURE 5. 1 Schematic view of the LED device, which consists of ZnO thin film on c-sapphire substrate, vertically aligned ZnO nanowires, ITO contacts and Ti/Au contacts.

5.3 Results and Discussion

Since this device is essentially the same device for photodector presented in chapter 4, the structure and electrical properties of this device can be found there. Electroluminescence(EL) was measured for this device. Fig. 5.2 shows the EL spectra of the device under different injection current. It is evident that near-band-edge emission at 380 nm is observed as a result of radiative recombination of more injected electrons and holes.

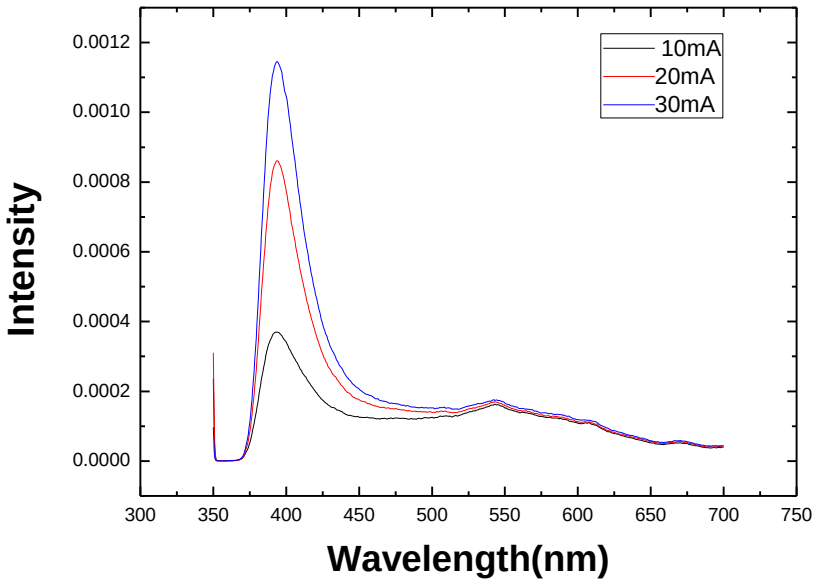

Fig. 5.2 EL spectra of the device under different injection current.

5.4 Conclusion

ZnO p-n homojunctions based on Sb-doped p-type nanowire arrays and n-type thin films were grown by the combination of CVD and MBE. The ZnO thin film/nanowire p-n junction was proved by EBIC profiling, I-V measurement, and field-effect

measurement. Evident UV emissions were observed under different current injection. This study not only proved that Sb doping can lead to p-type ZnO nanowires but also demonstrated an ultraviolet homojunction LEDs based on p-type nanowire array and n-type thin film.

5.5 References

[1] E. O. Kane, Phys. Rev. B **18**, 6849 (1978).

[2] C. Klingshirn,Phys. Status. Solidi. B **244**, 3027(2007).

[3] D. C. Look, Mater. Sci. Eng. B **80**, 383 (2001).

[4] S. Chu, J. H. Lim, L. J. Mandalapu, Z. Yang, L. Li, and J. L. Liu, Appl. Phys. Lett. **92**, 152103 (2008).

[5] H. Cao, Y. G. Zhao, H. C. Ong, S. T. Ho, J. Y. Dai, J. Y. Wu, and R. P. Chang, Appl. Phys. Lett. **73**, 3656 (1998).

[6] S. F. Yu, C. Yuan, S. P. Lau, W. I. Park, and G. Yi, Appl. Phys. Lett. **84**, 3241 (2004).

[7] S. Chu, M. Olmedo, Z. Yang, J. Y. Kong, and J. L. Liu, Appl. Phys. Lett. **93**, 181106 (2008).

[8]C. G. Van de Walle, Phys. Rev. Lett. **85**, 1012 (2000).

[9]D. K. Hwang, H. S. Kim, J. H. Lim, J. Y. Oh, J. H. Yang, S. J. Park, K. K. Kim, D. C. Look, and Y. S. Park, Appl. Phys. Lett. **86**, 151917 (2005).

[10] K. K. Kim, H. S. Kim, D. K. Hwang, J. H. Lim, and S. J. Park, Appl. Phys. Lett. **83**, 63 (2003).

[11] T. S. Jeong, M. S. Han, C. J. Youn, and Y. S. Park, J. Appl. Phys. **96**, 175 (2004).

[12]F. X. Xiu, Z. Yang, L. J. Mandalapu, D. T. Zhao, and J. L. Liu, Appl. Phys. Lett. **87**, 152101 (2005).

[13] L. J. Mandalapu, F. X. Xiu, Z. Yang, D. T. Zhao, and J. L. Liu, Appl. Phys. Lett. **88**, 112108 (2006).

[14] L. J. Mandalapu, Z. Yang, F. X. Xiu, D. T. Zhao, and J. L. Liu, Appl. Phys. Lett. **88**, 092103 (2006).

[15] C. H. Chen, S. J. Chang, S. P. Chang, M. J. Li, I. C. Chen, T. J. Hsueh, and C. L. Hsu, Appl. Phys. Lett. **95**, 223101 (2009).

[16] X. M. Zhang, M. Y. Lu, Y. Zhang, L. J. Chen, and Z. L. Wang, Adv. Mater. **21**, 2767 (2009).

[17] L. E. Greene, M. Law, D. H. Tan, M. Montano, J. Goldberger, G. Somorjai, and P. D. Yang, Nano. Lett. **5**, 1231 (2005).

Chapter Six

Electrically Pumped Waveguide Lasing from ZnO Nanowires

6.1 Introduction

Single-crystalline semiconductor nanowires have long been considered as an excellent candidate to realize small and cost-effective FP type lasers because of the optical feedbacks provided by the naturally formed flat facets in the ends of nanowires. Although optically pumped nanowire lasers are widely reported [1-10], only single cadmium sulfide (CdS) nanowire/Si heterojunction laser has been demonstrated in electrically driven way[11], and there lacks high-efficiency homojunction lasers. In ZnO, this is mainly due to the difficulty of controllable *p*-type doping [12-14]. As reliable *p*-type doping of ZnO keeps on progressing, more nanowire based optoelectronic device will certainly emerge, for example, *p*-*n* homojunction nanowire light emitting diode (LED) [14] and photodiode [15] have been realized recently. In this chapter, we report a homojunction diode, which consists of *p*-type Sb-doped ZnO nanowires on high-quality *n*-type ZnO film. Evident FP type UV lasing was demonstrated while gain/feedback mechanisms as well as laser emission profile were studied in detail.

6.2 Experimental Section

ZnO thin film growth: The *n*-type ZnO film was grown on a 2-inch *c*-plane sapphire substrate using plasma-assisted MBE. The growth began with a 1-minute growth of MgO for improving the subsequent ZnO film quality, followed by a regular ZnO buffer layer growth at 550 ºC for 8 minutes. The subsequent main ZnO film was grown at 700 ºC for

5 hours, yielding a total film thickness of around 1050 nm. The Zn effusion cell temperature was kept at 360 ºC with a beam flux on the order of 10^{-7} Torr. The oxygen plasma was generated by a radio-frequency (RF) system and the flow rate of oxygen is 5 standard centimeter cube per minute (sccm).

ZnO nanowire growth: The *c*-axis oriented ZnO thin film acts as both seed layer for ZnO nanowire growth as well as *n*-type component of the *p*-*n* junction light emitting device. The ZnO/*c*-sapphire sample was subsequently transferred to a CVD furnace for vapor-solid growth of Sb-doped ZnO nanowires. The sample was partially covered during the nanowire growth to expose the ZnO film for *n*-type contacts deposition.

The ZnO nanowires were grown by a quartz tube furnace system (Thermal Scientific Inc.) Zinc powder (99.999% Sigma Aldrich) in a glass bottle was placed in the center of the quartz tube. Sb powder (99.99% Sigma Aldrich) was put in an open glass boat. The boat was placed ~5 cm upstream to the zinc source. The ZnO film sample was kept 10 cm away from the zinc source on the down-stream side. The furnace was flown continuously by 1000 sccm nitrogen. The sources and sample were then heated to 650ºC at the temperature ramp rate of 30 ºC/min. After the desired temperature was reached, 200 sccm mixture gas of argon/oxygen (99.5: 0.5) was introduced to the quartz tube for ZnO nanowire growth. The growth was kept for 15 minutes.

Device fabrication

N-type contact: Au/Ti (100 nm/10 nm) contact was deposited on the n-type ZnO films

(the n-contact area was intentionally covered during nanowire growth). **Top ITO contact**: After ZnO nanowire formation, poly methyl methacrylate (PMMA) was spun on the sample to separate the bottom ZnO film and subsequent ITO top contact. The spin rate was 2000 rpm for 30 seconds, and this process was repeated for 5 times. After drying, the sample was put into a DC magnetron sputtering system. ITO target 99.99% was acquired from Sigma Aldrich. The growth was taken at RT and the pressure was maintained at 10^{-2} Torr. The sputtering power and time was 180 W and 10 minutes, respectively. The ITO glass slides (15~25 Ω/sq) for the reliable current feed through were acquired from Sigma Aldrich. The fabricated device has an area of about 5×10 mm^2.

EBIC measurement: EBIC profile measurements were conducted on the ZnO nanowire/ZnO film cross-sectional structure which was done by cleaving the sample. The measurement was carried out in a Philips XL30 SEM under a 30 kV electron beam accelerating voltage. EBIC signal line scans were recorded using homemade software. A Stanford Research System low noise current amplifier and a Keithley 2000 digital multi-meter were employed as digitizer.

PL and EL measurement: The system consists of an Oriel monochromator and a lock-in amplifier with a chopper. A 325 nm He-Cd laser was used as excitation source. A photo-multiplier tube was used to detect the device light emission, which is emanated out of ITO/glass electrode from the nanowires. The scan step in PL and EL was 0.3 nm. An external HP E3630A DC power supply was used to input current for EL measurement. To

record the far field lasing pattern, a Nikon Eclipse L200 microscope is equipped with a Sony DXC 970 CCD camera. For the optically pumped lasing demonstration, the system is built up by using UV enhanced objective (40X) and PI monochrometer equipped with Si CCD. The laser excitation source is an Nd: YAG pulse laser with output wavelength of 355 nm (3 ns pulse).

Scanning AES measurement: A PHI 700 Scanning Auger Nanoprobe system was used for Sb dopant profile distribution characterization. A reference sample grown at the same condition was used for characterization.

FDTD simulation

FDTD solution 6.5 (Lumerical Inc.) was used for simulation. The pumping source is a point transverse electric wave (380 nm ~400 nm) source located between the ZnO nanowire (center one) and ZnO film, which corresponds to the *p*-*n* junction active area. The diameter and length of the nanowire are 200 nm and 3.2 μm, respectively. The nanowire inter-distance is 400 nm. The thickness of ZnO film is 1.05 μm. A frequency-domain power monitor was used to record the emission profile over the simulation region.

6.3 Results and Discussion

Figs 6.1a and 6.1b show a schematic, and a photo of the device, respectively. The growth of the *p*-type ZnO nanowire/*n*-type ZnO film diode structure was done via seed-assisted growth scheme [16, 17]. First, a 1050 nm thick high-quality *n*-type ZnO seed film was grown

on *c*-plane sapphire substrate by plasma-assisted molecular beam epitaxy (MBE). SEM and x-ray diffraction (XRD) measurements were carried out to characterize the ZnO film. Top-view and side-view SEM images of the ZnO film are shown in Figs. 6.2 (a) and (b), respectively. The morphology of the thin film consists of multiple packed hexagonal columns, which originate from ZnO preferential growth along *c*-axis. The preferential growth is confirmed by XRD 2θ scan in Fig. 6.3, where distinct ZnO (0002) and (0004) peaks are clearly observed.

Electrical properties of the ZnO film were characterized by Hall effect measurement under a Van der Pauw configuration. To be consistent with the device sample, the ZnO film was annealed at 650ºC for 20 minutes. Electron concentration of $7.8\times10^{18}/cm^3$, mobility of 11.04 cm^2/Vs and resistivity of 0.07 Ωcm were obtained. The large carrier concentration guarantees good electron injection in the laser device.

Then, Sb-doped *p*-type nanowires were grown on top of the film by chemical vapor deposition (CVD). The *c*-axis of the ZnO nanowires perfectly follows the growth direction of the underneath film, resulting in highly-oriented vertical nanowires array (Fig. 6.1c and Fig. 6.4). The length and diameter of the nanowires are on average 3.2 μm and 200 nm, respectively.

The major merit of the device structure is the integration of the advantages from both MBE and CVD. MBE grows high-quality thin films but it is not practical to grow nanowires due to relatively low growth rate. On the other hand, CVD furnace synthesizes high-quality nanowires with fast growth speed but can hardly achieve controllable multi-segment nanowires growth with different conductivity types. Therefore the approach by

growing *p*-type nanowires in CVD on high-quality *n*-type films by MBE can solve this dilemma and produce controllable *p*-*n* homojunctions. The single-crystalline nature of ZnO nanowires was confirmed by high-resolution transmission electron microscopy (TEM) imaging analysis (Fig.6.5). The lattice spacing between the two atomic layers is measured to be 0.51 nm (Fig.6.5(a)). Fig. 6.5(b) is the selected area electron diffraction (SAED) pattern. These results suggest single crystalline nature of the nanowire.

Sb dopant incorporation was proved by x-ray photoelectron spectroscopy (XPS) spectrum in Fig. 6.1d, which shows a clear Sb $3d_{3/2}$ peak at 539.5 eV. This peak position suggests that the Sb atoms substitute Zn atoms (Sb_{Zn}) [18]. Sb distribution along the nanowires was also proved by Auger electron spectroscopy (AES). AES line scan was done on a single nanowire of a reference sample grown at the same Sb-doping condition as the device sample. The result is shown in Fig. 6.6. The Sb signal slowly decreases from 1.8% at the top to 1.3% at the bottom.

AES spectra were recorded on two individual points of one nanowire on the same sample as shown in Fig. 6.7a. The measurement points are marked “1” and “2” and corresponding AES spectra are shown in Fig. 6.7b. The two points show Sb signals of 1.7 % and 1.2 %, respectively, suggesting the incorporation of Sb, which is in consistent with XPS result shown in Fig. 6.1d. Higher Sb concentration in the upper part of nanowires may be due to the incorporation of Sb after growth when the furnace is still hot for a short period of time.

The lasing of the nanowires was firstly demonstrated via optical pumping. Fig. 6.1e shows the lasing spectra at different pumping power. Equal-distance peaks with

separation of ~2.4 nm are observed (solid arrows). It is also noticeable that at higher pumping powers, additional modes indicated by dashed arrow begin to show up due to the excitation of the adjacent nanowires with slightly different length. The threshold power is ~180 kW/cm^2 from the plot of the intensity as a function of pumping power in the inset of Fig. 6.1e. The density of electron hole pairs (n_p) produced by the optical pumping can be calculated as: $n_p=I_{exc}\tau/h\omega l$ [19], where I_{exc} is the excitation power, τ is the spontaneous emission life time (τ varies [20] and is assumed to be 300 ps [21]) and l is the diffusion length (~2 μm [22] from top excitation). The analysis roughly gives an n_p of 5.1×10^{17}/cm^3 at the threshold.

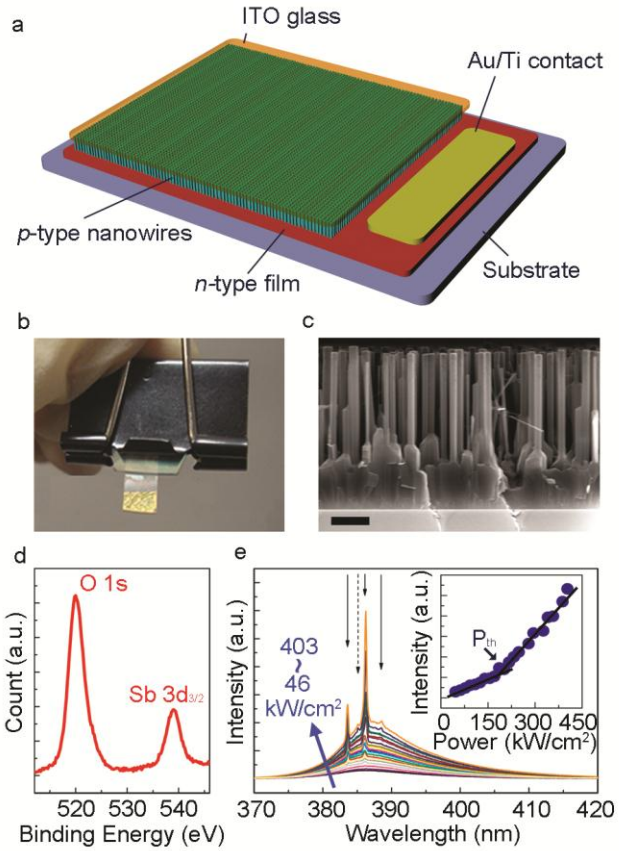

FIGURE 6.1 Structure and material properties of ZnO nanowire/film laser device. (a), Schematic of the laser device that consists of *n*-type ZnO thin film on *c*-sapphire substrate, *p*-type vertically aligned ZnO nanowires, ITO contact and Au/Ti contact. (b), Photo image of the device. (c**)**, Side-view SEM image of the device structure showing ZnO thin film and nanowires. Scale bar is 1 μm. (d), XPS spectrum of the Sb-doped ZnO nanowires array. (e), RT optically pumped lasing spectra from 46 kW/cm^2 to 403 kW/cm^2

with average ~20 kW/cm^2 step. Solid arrows denote equal-distance lasing peaks and the spacing of 2.4 nm is extracted. Inset shows the integrated spectra intensity as a function of pumping power density, solid lines are used to show the threshold P_{th} (~180 kW/cm^2).

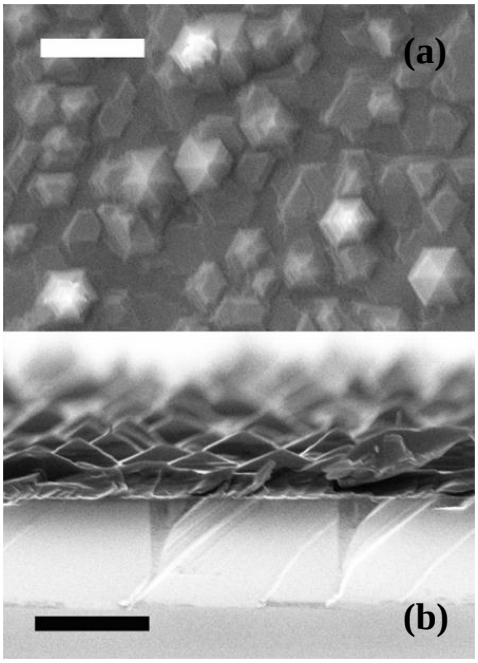

Figure 6.2. (a) Top-view, and (b) Side-view SEM image of the ZnO thin film grown by MBE.

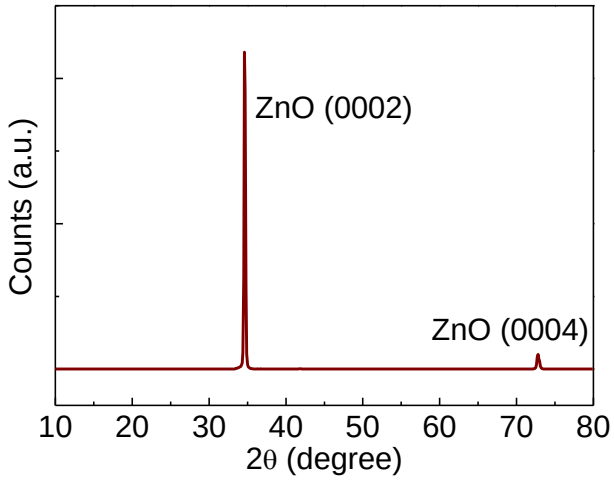

Figure 6.3. XRD scan of the ZnO thin film grown by MBE.

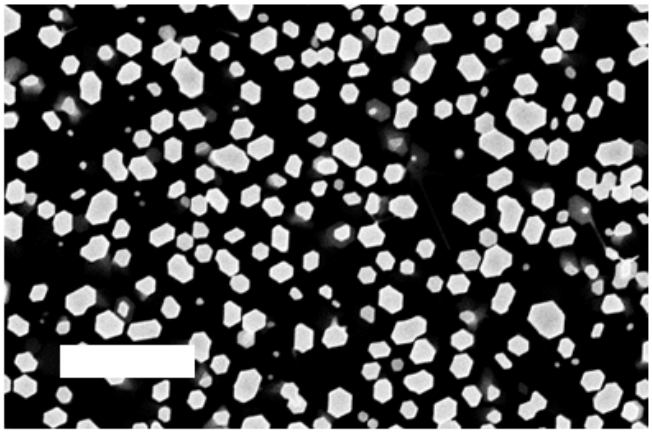

Figure 6.4. Top-view SEM image of the nanowire array. Good vertical alignment of nanowires is evident. Scale bar: 1 μm.

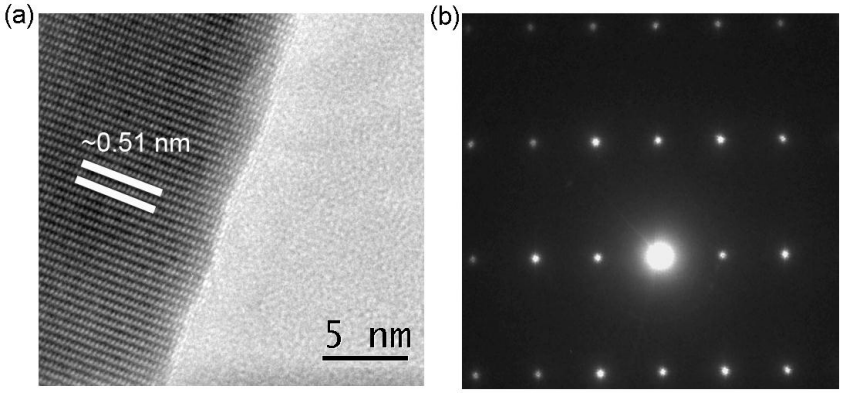

Figure 6.5. (a) TEM image of the Sb-doped ZnO nanowire. (b) SAED pattern.

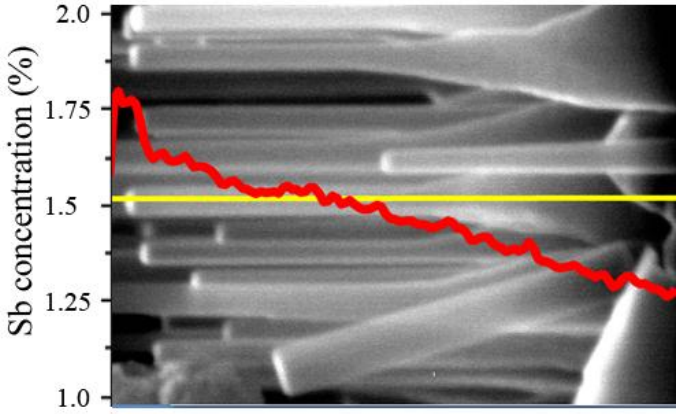

Figure 6.6. Sb profile determined by AES scan superimposed on SEM image. The yellow line is the scan line.

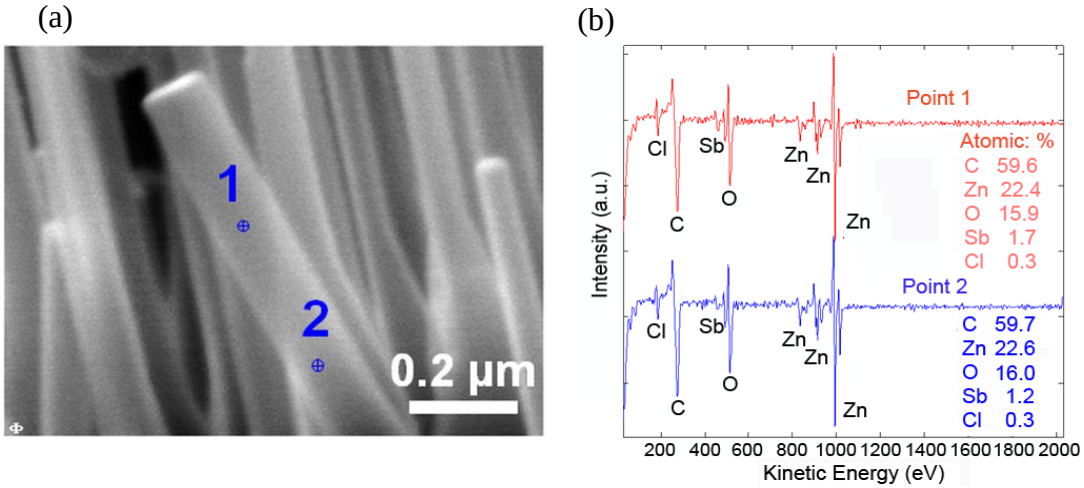

Figure 6.7. (a) AES measurement points on the nanowire in SEM image. (b) The corresponding AES spectra and elemental analysis result.

In Fig. 6.8a, current-voltage (I-V) characteristic exhibits rectifying diode behavior. However, the large reverse current is related to the formation of ITO/Sb-doped ZnO nanowires metal-semiconductor junction, which is in series to ZnO *p-n* homojunction. The formation of ZnO homojunction between the nanowires and film was investigated by electron beam induced current (EBIC) profiling [23, 24]. To facilitate EBIC experiment, silver paste was utilized to contact the top ends of nanowires. Fig. 6.8b shows the EBIC profile superimposed on the cross-sectional SEM image. The EBIC signal forms a peak across the nanowire/film junction due to the drift of electron-beam generated electrons and holes under the influence of built-in electric field, indicating the formation of *p-n* junction. The second peak on the right side is related to the additional non-equilibrium

electron collection from the ZnO/ITO/silver paste contacts. *P*-type conductivity of the ZnO nanowires can be proved by field-effect measurement (Figs. 6.9 and 6.10). Another batch of ZnO nanowires were grown at the same growth condition. The nanowires were transferred onto a SiO_2/p^+-Si substrate for nanowire FET device fabrication. The thickness of the SiO_2 layer is 300 nm. Standard photolithography techniques were used to define the micro-contacts onto the nanowires. The SEM image in the inset of Fig. 6.9 shows successful placing of Au/Ni (100 nm/20 nm) contacts on the ZnO nanowire. Field effect measurement was achieved by using Si substrate as the global back gate. Fig. 6.9 shows I_{DS} vs V_G curve under different drain voltages. The results suggest that the Sb-doped ZnO nanowires exhibit *p*-type behavior under gate voltage ranging from -10 V to 20 V, that is, the conductance of ZnO nanowire decreases with the increase of positive gate voltage. Fig. 6.10 shows I_{DS}-V_{DS} output characteristics of the nanowire FET under a gate bias of 10 V, 0 V, and -10 V, respectively. The result agrees with the transfer characteristics and further confirms the *p*-type behavior of the nanowires. Some electrical transport properties were extracted using simple nanowire FET model. Capacitance of the system was calculated to be 2.22×10^{-16}F by $C = 2\pi\varepsilon_0\varepsilon_{SiO2}\mathrm{L}/\ln\left(\frac{4h}{d}\right)$, where L = 1.8 μm is the nanowire length between contacts, h=300 nm is the thickness of SiO_2 and d ~ 200 nm is the nanowire diameter. Hole concentration can be estimated by $\rho = V_{th}C/q\pi(\frac{d}{2})^2\mathrm{L}$, where q is the electron charge, V_{th} is the threshold voltage obtained from I_{DS}-V_G curve. As a result, hole concentration of $4.5\times10^{17}/cm^3$ to $2.5\times10^{18}/cm^3$ was extracted and the electrical properties are comparable to those of the *p*-type ZnO nanogenerators [12]. In the

meantime, carrier mobility was determined to be 0.005 to 0.03 cm^2/Vs by $g_m = \mu C V_{DS}/L^2$, where g_m is the transconductance of the FET. It should be noted that the mobility value here is actually at the low bound limit of the real mobility since the non-ohmic contacts between the metal and nanowire may bring large series resistance. Moreover, the nanowire device was wire bonded onto TO5 can and loaded in a cryostat for temperature-dependent I_{DS}-V_{DS} measurement. The results from 9K to 300K are shown in Fig. 6.11. The current intensity only changes by a factor of about 3 from RT to 9K, indicating a degenerate doping property, which is commonly observed in doped ZnO nanowires and can potentially give rise to efficient hole injection for lasing. In addition, the *p*-type behavior of the nanowires can also be confirmed optically by low temperature PL. PL spectra of both undoped and Sb-doped ZnO nanowires at 9K are shown in Fig. 6.12. The spectrum of the undoped ZnO nanowires shows a dominant neutral-donor-bound exciton (D^0X) peak at 3.361 eV, which is commonly assigned to I_8 transition in ZnO. The peak at 3.321 eV was identified as two-electron-satellite (TES) transition of I_8. 3.300 eV, 3.229 eV and 3.157 eV peaks are attributed to phonon replicas of the free exciton A (FX_A) emission.

In contrast, Sb-doped ZnO nanowires spectrum shows distinct neutral-acceptor-bound exciton (A^0X) peak at 3.350 eV. In addition, this peak becomes significantly wider than D^0X in the undoped ZnO nanowire, which is due to extensive dopant incorporation. The broad emission around 3.0 eV is related to zinc vacancies, which is also a signature of Sb-doped ZnO thin films. The PL analysis suggests that the Sb-doped ZnO has shallow acceptor induced energy levels, which result in the *p*-type behavior of the nanowires.

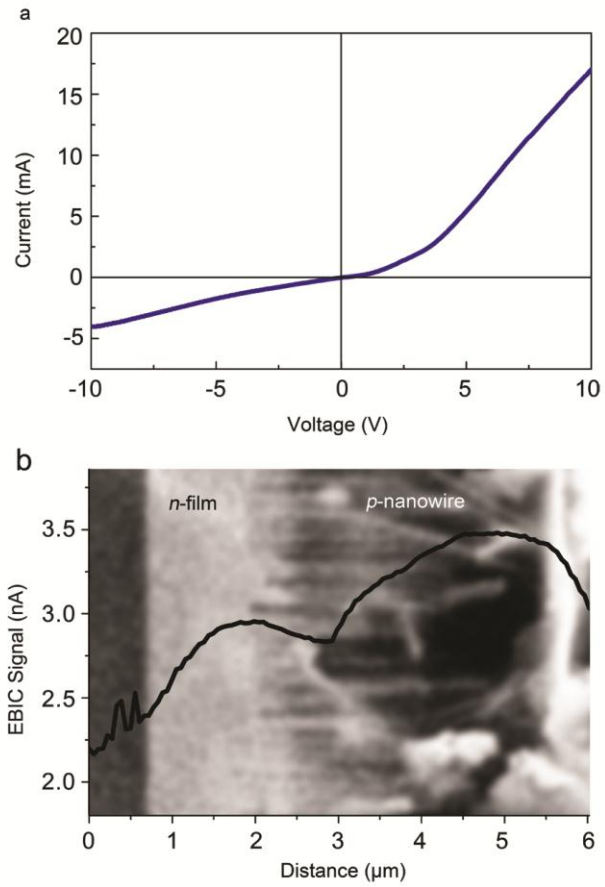

FIGURE 6.8 I-V property and evidence of the formation of ZnO nanowire/film *p-n* junction. (a), I-V characteristic of the ITO/ZnO nanowire/ZnO film laser device. Positive bias is applied on the ITO side. (b), Electron beam induced current (EBIC) profile superimposed on the side-view SEM image of the cleaved device.

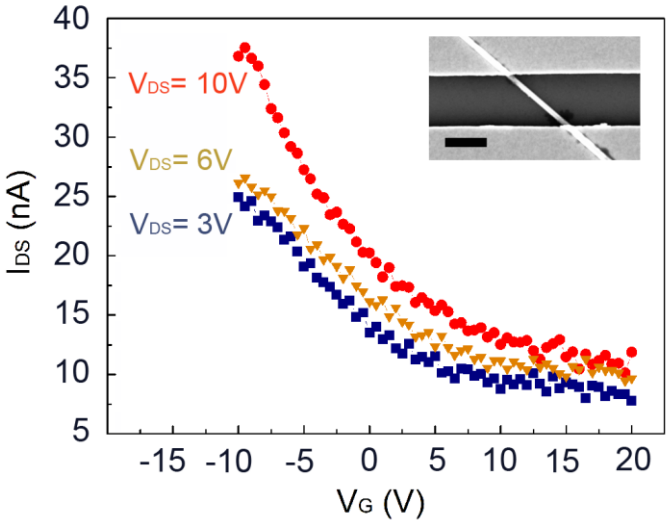

Figure 6.9. Drain-source current (I_{DS})-gate voltage (V_G) at drain-source voltage (V_{DS}) of 3 V, 6 V and 10 V, respectively. The decrease of I_{DS} with V_G represents typical *p*-type FET characteristics. Inset is a SEM image of a single nanowire FET. Scale bar is 1 μm.

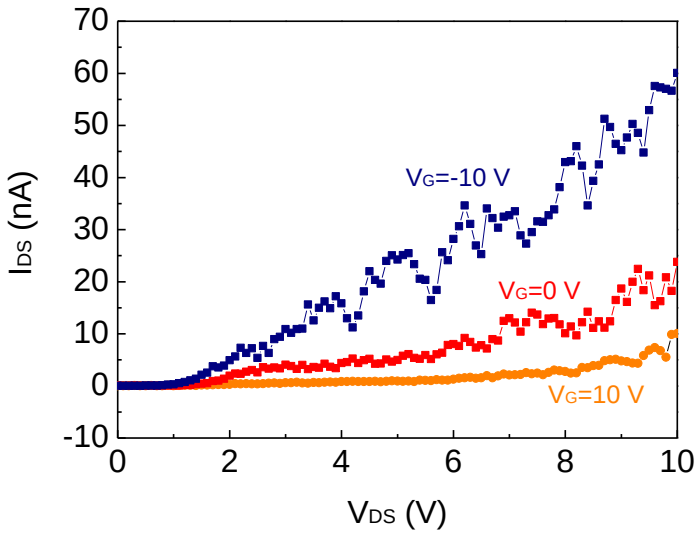

Figure 6.10. I_{DS}-V_{DS} curve of the ZnO nanowire FET under different gate voltages.

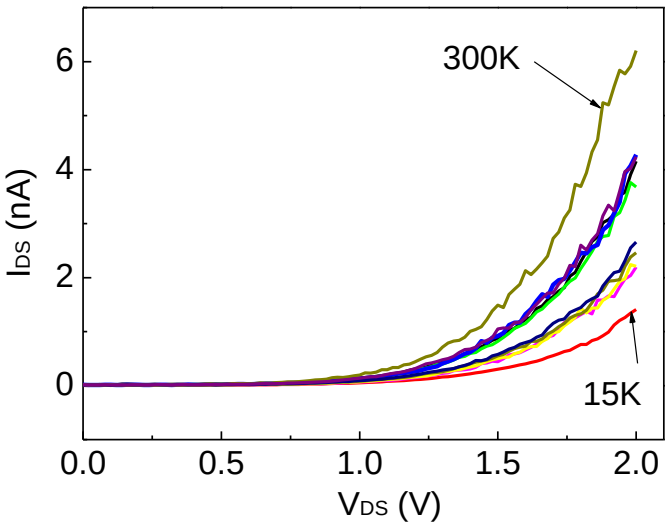

Figure 6.11. I_{DS}-V_{DS} curves of the ZnO nanowire FET from 15 K to 300K. The gate voltage was 0 V.

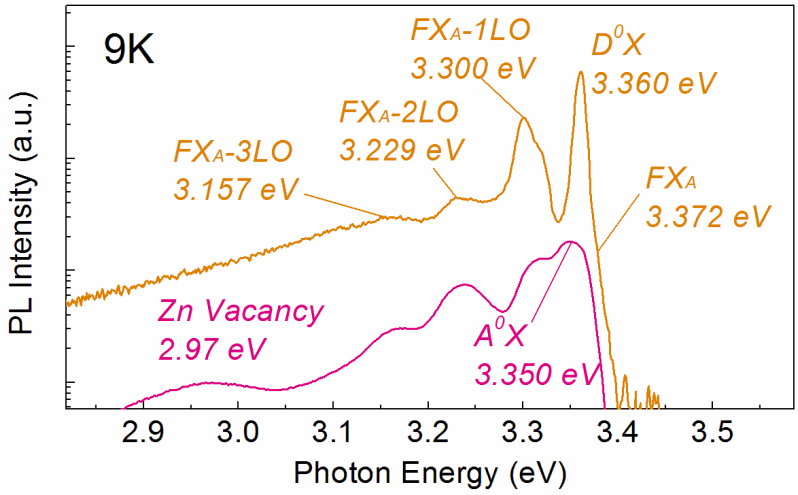

Figure 6.12. 9K PL spectra of undoped ZnO nanowires (top curve) and Sb-doped ZnO nanowires (bottom curve).

Electroluminescence (EL) characterizations were performed to demonstrate the lasing action. The left column of Fig. 6.13 shows EL spectra under injection current from 20 mA to 70 mA. Under low injection currents from 20 mA to 40 mA, only free exciton spontaneous emissions centered at around 385 nm are observed. As the pump current reaches a threshold of around ~50 mA, drastic sharp emissions with line-width as narrow as 0.5 nm emerge from the single-broad emission around 385 nm, which indicates that the gain is now large enough to enable cavity mode to start lasing. Further increase of the injection current stimulates the onset of lasing in additional nanowires with slightly different length, resulting in the increase of the number of lasing peaks. Stable, quasi-equal distance pattern of lasing peaks can be extracted with reasonable wavelength deviation. The average spacing between modes ($\Delta\lambda$) is 2.52 nm for selected peaks denoted by arrows in Fig. 6.13, which is close to the spacing in optical pumping from Fig. 6.1e (2.4 nm). The spacing $\Delta\lambda$ for a FP cavity is given by: $\Delta\lambda = \lambda^2 \left[2L\left(n - \lambda\frac{dn}{d\lambda}\right)\right]^{-1}$[11], where n=2.5 is the refractive index of ZnO and $dn/d\lambda = -0.015\ nm^{-1}$ denotes the dispersion relation for the refractive index. For 4.2 μm cavity between the top end of the ZnO nanowire and the bottom ZnO film/sapphire interface determined by SEM imaging, $\Delta\lambda$ is calculated to be 2.95 nm, which is in close agreement with the observed experimental values. To verify the FP lasing mechanism for the sample described in the above text from a different angle, another sample with similar structure was fabricated. The total thickness of this sample is ~ 10 μm as shown in Fig. 6.14. According to the line spacing

formula $\Delta\lambda = \lambda^2 \left[2L\left(n - \lambda\frac{dn}{d\lambda}\right)\right]^{-1}$, the line spacing for this resonant cavity is 1.24 nm. EL spectrum of this device under an injection current of 30 mA is shown in Fig. 6.15. The spectrum shows multiple lasing peaks that are similar to the device described in the main text. The average peak spacing is ~1.5 nm, which is close to the calculated value of 1.24 nm.

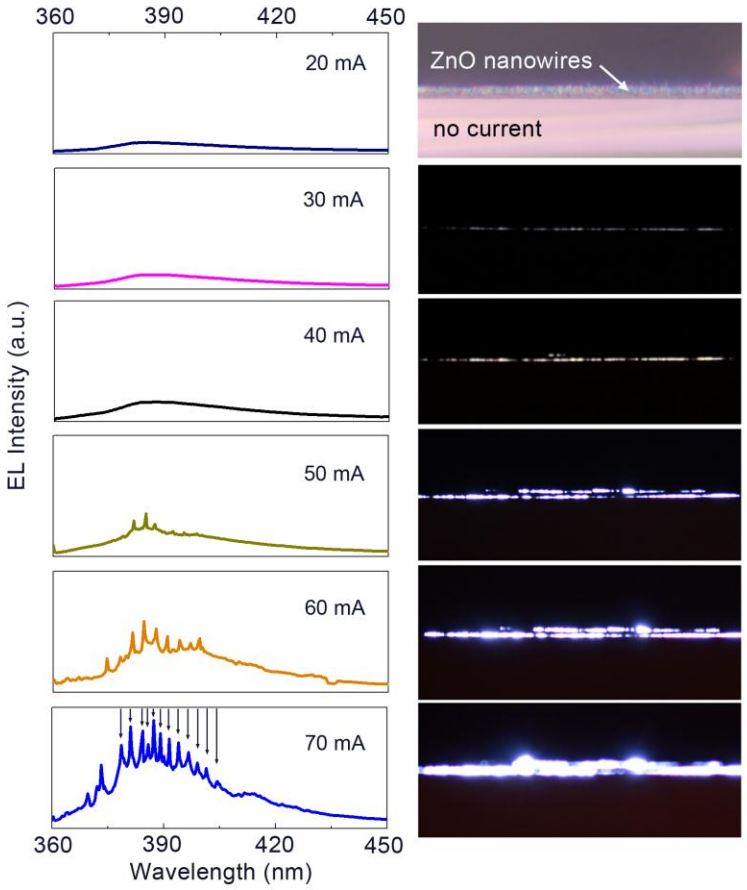

FIGURE 6.13 Laser emission characterizations. Left column: EL spectra of the laser device operated at between 20 mA and 70 mA. Above 50 mA, the lasing characteristics are clearly seen. Arrows in 70 mA spectrum represent quasi-equal distance peaks. Right column: Side-view optical microscope images of the lasing device. Each one corresponds to the EL spectrum in the left column. The first image was taken with lamp illumination and without current injection.

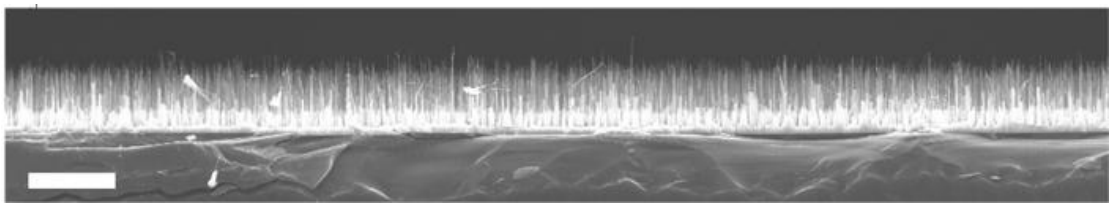

Figure 6.14. Side-view SEM image of the longer cavity sample. Scale bar is10 μm.

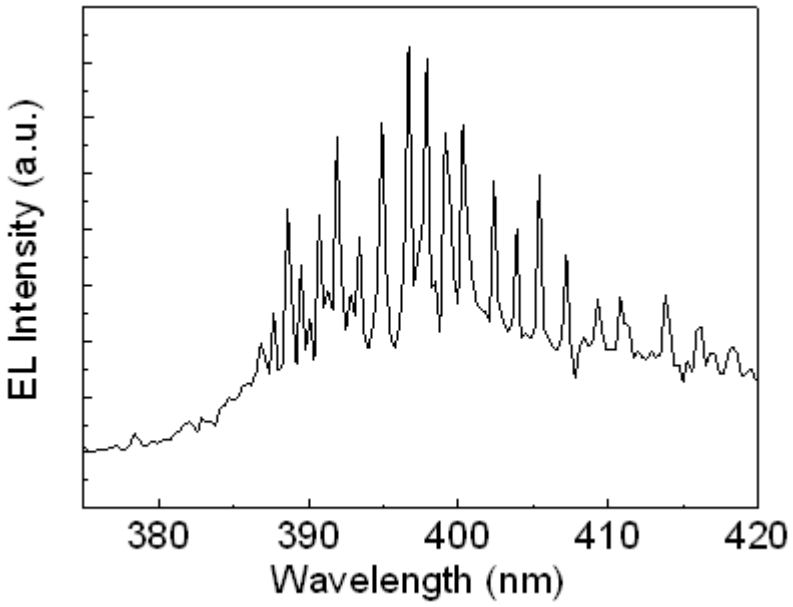

Figure 6.15 EL spectrum of the long cavity device operated at 30mA.

In addition to the spectra features, the right column of far-field microscope images in Fig. 6.13 shows direct evidence of nanowire FP type lasing. First, side-view ZnO nanowires array can be seen at the center of the first image. Then the illumination lamp was switched off and emission light was recorded for the biased device from 30 mA to 70 mA. Under the excitation of 30 mA, distinct light emission shows up to form a stripe

close to the bottom of the nanowires/thin film interface, indicating that electrically pumped light emission starts near the *p*-*n* junction active region rather than at the ITO/ZnO nanowire interface. With the increase of the injection current, the light from the top ends of the nanowires emerges. As the pumping current increases to 60 mA or 70 mA, this behavior becomes very prominent with bright light spot pairs at the two ends of the nanowires. This striking phenomenon is a strong proof of longitudinal lasing modes in a waveguide that has been constantly observed in nanowire lasing[3, 11, 26].

The integrated lasing spectrum intensity is plotted against the injection current value, as shown in Fig. 6.16. Dash line is plotted to guide the eyes, showing evident threshold current of about 48 mA. The gain/feedback mechanism of this nanowire/thin film FP laser is shown in the left inset of Fig. 6.16. It can be inferred that the gain length is determined by the minority carrier diffusion lengths in *p*-type (L_n ~2 μm [22]) nanowire and *n*-type ZnO film (L_p ~200 nm [27]), as well as the width of the space charge region (<100 nm). Thus the total gain length is ~2.3 μm. In FP laser, threshold gain (G_{th}) is given as [26]

$$G_{th} = \frac{1}{2L} \ln\left(\frac{1}{R1 \times R2}\right),$$

where R1 and R2 are reflectivities on the two ends of the cavity, which are 0.04 for sapphire/ZnO and 0.09 for ZnO/ITO/glass. L is the gain length. Calculation leads to G_{th}~1.2×10^4 cm^{-1} for this laser. On the other hand, optically pumped lasing (Fig. 6.1e) needs reduced G_{th}~5.6×10^3 cm^{-1} mainly due to longer L (4.2 μm) and larger reflectivity at ZnO/ITO/air (0.2). Excited carrier density of $5.1\times10^{17}/cm^3$ was estimated at the threshold for optically pumped lasing in the previous paragraph. So it is reasonable to

assume that higher carrier densities, for example $>1.0\times10^{18}/cm^3$ are needed in the electrically pumping case because of the larger G_{th}. These numbers are around or larger than calculated Mott density of ZnO [19, 28] therefore electron-hole plasma (EHP) rather than exciton-exciton interaction may dominate the lasing process. Using $n_p=I_{th}\tau/eV_{gain}$ [19], where I_{th} is threshold current, and $V_{gain}=L\times S$ (S: nanowire cross-section area) is the volume of the gain region, threshold current in each lasing nanowire I_{th} is determined to be > 39 μA. This is comparable with the threshold current of 200 μA in CdS nanowire laser [11]. This situation can be readily achieved due to the fact that initial current crowding effect will allow a handful of nanowires among those tightly connected with ITO/glass contacts to meet the threshold gain and lase, and further increase of injection currents involve more nanowires to emit lasing.

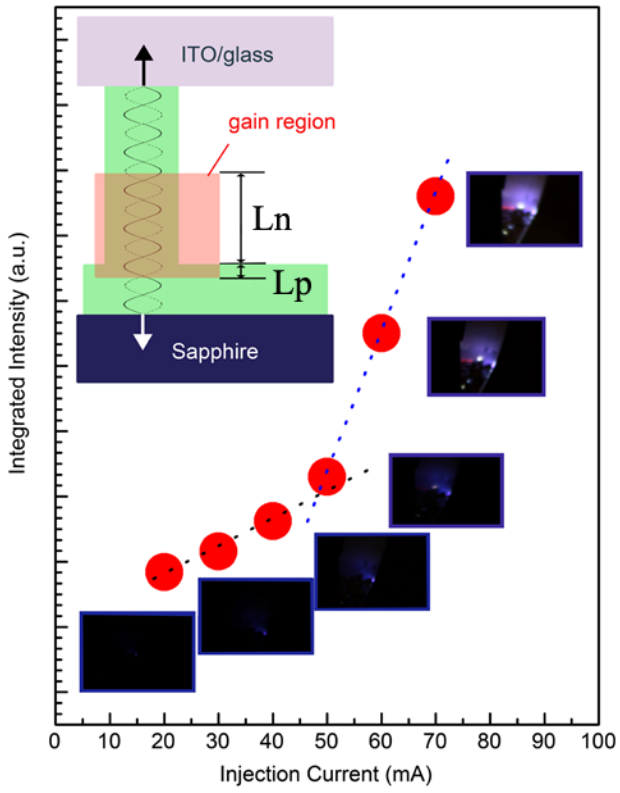

FIGURE 6.16 Lasing threshold gain/feedback properties. Integrated spectrum intensity as a function of injection current. Dashed line is used to guide the eyes. Right inset shows camera images that correspond to the emission pattern along the nanowire length direction at each of the injection current. Left inset shows the gain feedback diagram of the ZnO nanowire/thin film laser cavity. The laser gain area is defined by the diffusion length L_n and L_p as marked red in the figure.

Under corresponding injection currents, the lasing images taken from the nanowire length direction are displayed in the right inset of Fig. 6.16. Blue-purple light becomes significantly brighter as the pumping is above threshold. The evolution of the spatial distribution of the emissions was studied by FDTD simulations. The simulation/measurement environment is schematically illustrated in Fig. 6.17. The simulated spatial distribution of the emission is displayed in Fig. 6.17b and far-field emission intensity as a function of angle with respect to the nanowire length direction is shown in Fig. 6.17c. The result suggests that the nanowire laser device emits intense light close to the nanowire length direction; in the meantime, the light spreads in a concentrated conic shape with angular oscillation. The simulated pattern follows well with previous nanowire laser studies [3, 26, 29-30]. Experimental far-field emission values (blue square symbols) are shown in Fig. 6.17c. The result is in close agreement with the simulated data of the far-field pattern, further proving the waveguide mode emission.

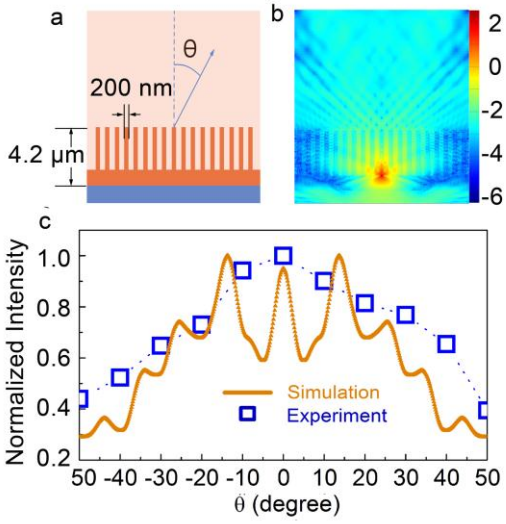

FIGURE 6.17 Far-field pattern of the light emission. (a), Schematic view of the FDTD

simulation/measurement environment. The area has a dimension of 9×10 μm. **(**b), Simulated spatial distribution of the light (385 nm) intensity. (c), Angle distribution of the far-field emission patterns. X-axis is the emission angle θ with respect to the nanowire growth direction and y-axis is the normalized emission intensity. Orange curve shows the simulation result and blue square symbols originate from the results from EL measurement by rotating the device with respect to the nanowire length direction.

6.4 Conclusion

We achieved the electrically pumped ZnO nanowire diode lasers using *p*-type Sb-doped ZnO nanowires and *n*-type ZnO film. FP type UV lasing was demonstrated at RT with good stability. The work on ZnO UV lasing may enable many potential applications. Future work is needed to further optimize the laser performance. For examples, the top contact with the *p*-type nanowire might be engineered to offer both good optical transparency and low electrical resistivity; Heterojunction nanowire diode structures may be used to achieve stronger power output.

6.5 References

1. Yan, R., Gargas, D., & Yang, P. Nanowire photonics. *Nature. Photon*. **3**, 569-576 (2009).
2. Huang, M. H. *et al*. Room-temperature ultraviolet nanowire nanolasers. *Science*, **292**, 1897-1899 (2001).
3. Vugt, L. K. V., Rühle, S., & Vanmaekelbergh, D. Phase-Correlated Nondirectional Laser Emission from the End Facets of a ZnO nanowire. *Nano Lett*. **6**, 2707-2711 (2006).
4. Zhou, H. *et al*. Ordered, uniform-sized ZnO nanolasers arrays. *Appl. Phys. Lett*. **91**, 181112 (2007).
5. Kwok, W. M. *et al*. Influence of annealing on stimulated emission in ZnO nanorods. *Appl. Phys. Lett*. **89**, 183112 (2006).
6. Gargast, D. *et al*. Whispering gallery mode lasing from ZnO hexagonal nanodisks. *ACS Nano*. **4**, 3270-3276 (2010).
7. Ma, X. Y. *et al*. Room temperature electrically pumped ultraviolet random lasing from ZnO nanorod arrays on Si. *Opt. Express*, **17**, 14426-14433 (2009).
8. Liang, H. K., Yu, S. F., & Yang, H. Y. Directional and controllable edge-emitting ZnO ultraviolet random laser diodes. *Appl. Phys. Lett*. **96**, 101116 (2010).
9. Zhu, H. *et al*. Low threshold electrically pumped random lasers. *Adv. Mater.* **22**, 1877-1881 (2010).
10. Chu, S., Olmedo, M., Kong, J. Y., Yang, Z., & Liu, J. L. Electrically pumped ultraviolet ZnO laser diode. *Appl. Phys. Lett*. **93**, 181106 (2008).

11. Duan, X. F., Huang, Y., Agawal, R., & Lieber, C. M. Single-nanowire electrically driven lasers. *Nature* **421**, 231 (2001).

12. Lu, M. P. *et al.* Piezoelectric nanogenerator using *p*-type ZnO nanowire arrays. *Nano Lett.* **9**, 1223-1227 (2009).

13. Tsukazaki, A. *et al.* Repeated temperature modulation epitaxy for *p*-type doping and light-emitting diode based on ZnO. *Nature. Mater*. **4**, 42-46 (2005).

14. Chen, M. *et al*. Near UV LEDs made with in situ doped *p*-*n* homojunction ZnO nanowire arrays. *Nano Lett*. **10**, 4387-4393 (2010).

15. Wang, G. *et al*. ZnO homojunction photodiodes based on Sb-doped p-type nanowire array and n-type film for ultraviolet detection. *Appl. Phys. Lett*. **98**, 041107 (2011).

16. Greence, L. E. *et al.* General route to vertical ZnO nanowire arrays using texured ZnO seeds. *Nano Lett.* **5**, 1231-1236 (2005).

17. Wu, Y. W., Yeh, C. C., & Ting, J. M. Effects of seed layer characteristics on the synthesis of ZnO nanowires, *J. Am. Ceram. Soc*. **92**, 2718-2723 (2009).

18. Izquierdo, R., Sacher, E., & Yelon, A. X-ray photoelectron spectra of antimony oxides. *Appl. Surf. Sci.* **40** 175-177 (1989).

19. Klingshirn, C., Hauschild, R., Fallert, J. & Kalt, H. Room-temperature stimulated emission of ZnO: alternatives to excitonic lasing. *Phys. Rev. B* **75**, 115203 (2007).

20. Hauschild, R., Priller, H., Decker, M., Kalt, H., & Klingshirn, C. The exciton polariton model and the diffusion of excitons in ZnO analyzed by time-dependent photoluminescence spectroscopy. *Phys. Status Solidi C* **3**, 980-983 (2006).

21. Reynolds, D. C. *et al*. Time-resolved photoluminescence lifetime measurements of the Γ_5 and Γ_6 free excitons in ZnO. *J. Appl. Phys.* **88**, 2152 (2000).

22. Lopatiuk-Tirpak, O. et al. Studies of minority carrier diffusion length increase in p-type ZnO: Sb. *J. Appl. Phys*. **100**, 086101 (2006).

23. Hoffmann, S. *et al.* Axial *p-n* junctions realized in Silicon nanowires by ion implantation, *Nano Lett.* **9**, 1341-1344 (2009).

24. Chernyak, L. *et al.* Electron beam induced current profiling of ZnO *p-n* homojunctions. *Appl. Phys. Lett.* **92**, 102106 (2008).

25. Salfi, J., Philipose, U., Aouba, S., Nair, S. V., & Ruda, H. E. Electron transport in degenerate Mn-doped ZnO nanowires. *Appl. Phys. Lett.* **90**, 032104 (2007).

26. Johnson, J. C., Yan, H. Q., Yang, P. D., & Saykally, R. J. Optical cavity effects in ZnO nanowire lasers and waveguides. *J. Phys. Chem. B.* **107**, 8816-8828 (2003).

27. Soudi, A., Dhakal, P., and Gu, Y. Diameter dependence of the minority carrier diffusion length in individual ZnO nanowires. *Appl. Phys. Lett*. **96**, 253115 (2010).

28. Versteegh, M. A. M., Kuis, T., Stoof, H. T. C., Dijkhuis, J. I. Ultrafast screening and carrier dynamics in ZnO: theory and experiment. *arXiv: 1012.3600* (2010).

29. Friedler, I. *et al.* Solid State single photon sources: the nanowire antenna. *Opt. Express*. **17**, 2095-2110 (2009).

30. Zimmler, M. A., Bao, J., Capasso, F., Muller, S., & Ronning, C. Laser action in nanowires: observation of the transition from amplified spontaneous emission to laser oscillation. *Appl. Phys. Lett.* **93**, 051101 (2008).

Chapter Seven

Lasing Mechanism and Gain Calculation of ZnO

7.1 Lasing Mechanism

It has been generally mentioned in literature that the large exciton binding energy of 60 meV will lead to exciton-exciton scattering process (E-E), which can further result in high optical gain and low threshold lasers. Population inversion is readily achieved when two excitons exist in a system, leading to so called threshold-less lasing. If the pumping leads to a carrier density higher than the Mott density, the Coulomb interaction between electrons and holes is screened and excitons will condensate to electron-hole plasma. Generally the transition between excitonic processes to form electron hole plasma (EHP) process is continuous and determined by the pumping intensity. An inverted EHP can also give laser gain. In other words, the lasing in a given laser device can result from both E-E and EHP mechanism. After further studies as seen below, we tend to believe that our lasing mechanism is EHP lasing.

Table 7.1 lists reported lasing in typical ZnO nanostructures (optical pumping), and suggested lasing mechanisms.

Lasing mechanism (reference no.)	Cavity type/Nanostructure type	Lasing threshold
E-E [1]	FP/Nanowire	40 kW/cm^2 (70 nJ/cm^2)
EHP [2]	FP/Nanowire	~1 mJ/cm^2
EE [3]	WGM/Microwire	180 kW/cm^2
EHP [3]	WGM/Microwire	380 kW/cm^2
E-E [4]	FP/Nanobelt	350 kW/cm^2
EHP [5]	Random/Nanoneedle	250 kW/cm^2
EHP [6]	WGM/Microwire	160 kW/cm^2
EHP [7]	FP/Nanorod	~410 kW/cm^2
E-E [8]	FP/Nanowire	200 μJ/cm^2

From the table above, it is evident that the lasing threshold for both E-E and EHP varies on a wide range. Although EHP in principle requires higher amount of pumping than E-E, the threshold also depends on the Q factor, cavity loss, material quality, etc. The situation is complicated and highly controversial. One may argue that once the threshold is very low, for example, smaller than the lowest one of 40 kW/cm^2 listed in the table, it may be safe to claim E-E mechanism. However, the EHP lasing in GaN nanowires was found to need a pumping threshold as low as 22 kW/cm^2 [9]. So low threshold pumping density cannot be automatically linked to E-E whereas threshold

carrier density has to be calculated and analyzed to address the mechanism.

To help clarify the lasing mechanism in the present ZnO nanowires/thin film structure, we carried out optical pumping at pumping densities. 7.1 shows the results.

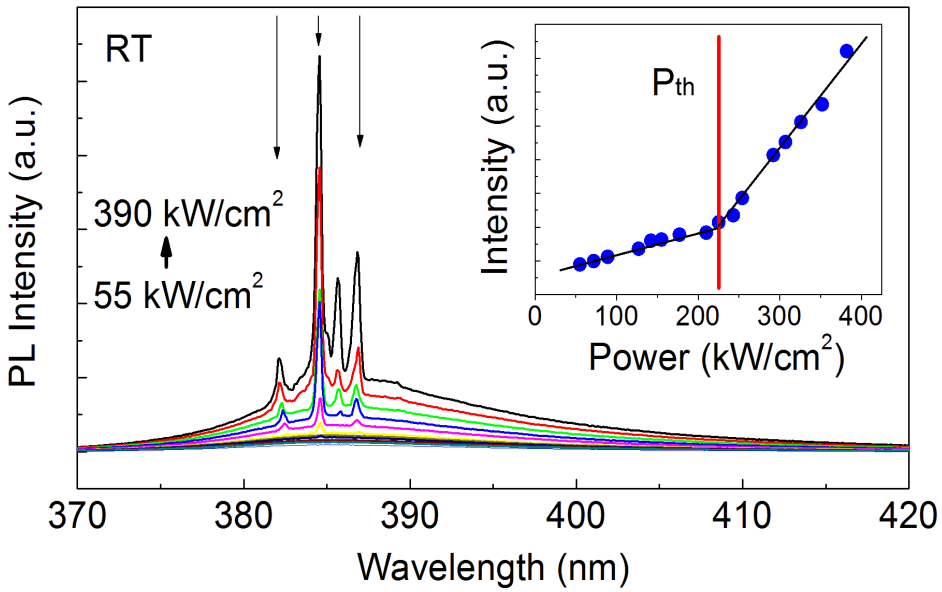

Figure 7.1 PL spectra of the sample. Excitation area: 1×10^{-5} cm^2. Threshold: 230 kW/cm^2.

Figure 7.1 shows the lasing action with a pumping area of 1×10^{-5} cm^2. The threshold pumping power is 230 kW/cm^2. It is also evident that with higher pumping density, new lasing modes from additional nanowires emerge, as marked with dashed arrow.

The fact that the lasing threshold density is slightly larger for a much larger excitation area rules out random lasing mechanism here, because in random lasing, larger area leads to smaller threshold pumping density [9-11]. Based on the line spacing of the lasing peaks of ~2.4 nm, FP type lasing is evident. Although the gain/feedback is slightly different between optical pumping and electrical pumping, the demonstration of clear optically pumped FP lasing is an indication of feasibility of FP lasing in the electrically pumped case.

The density of electron hole pairs produced by the optical pumping can be calculated as: $n_p=I_{exc}\tau/h\omega l$ [12], where n_p is the density of electron hole pairs, I_{exc} is the excitation power (230 kW/cm^2), τ is the spontaneous emission life time and l is the diffusion length (~2 μm from top excitation [12]). τ was reported as 100 ps, however it varies with a wide range[13-16], for example, Klingshirn *et al* used 300 ps in [12]. If we vary the decay time from 100 ps to 500 ps, n_p is calculated to be $1.9\times10^{17}/cm^3$ to $9.5\times10^{17}/cm^3$.

To determine the lasing mechanism, we need to compare the lasing threshold density and Mott density. The Mott density in ZnO has recently been calculated to be about $1.5\times10^{18}/cm^3$ using quantum many-body theory [17]. An earlier theoretical work by Klingshirn *et al* gave a smaller value of $5\times10^{17}/cm^3$ [12]; in their paper, they also calculated the carrier density in the nanowires in the paper published in Science [1] and found out that the electron-hole pair density at the threshold was $2\times10^{17}/cm^3$. Although

this number is smaller than the value of the Mott density of $5\times10^{17}/cm^3$, Klingshirn *et al* suggested the lasing mechanism of the optically pumped nanowire laser in [1] is still less likely to be E-E for the large damping of excitons at room temperature, which is quite reasonable. The carrier densities of the present optically pumped nanowire devices are on the order or above the density of $2\times10^{17}/cm^3$. Considering the above analysis, the lasing mechanism in this device is also less likely to be E-E, so we now agree that the lasing mechanism of the present device is most likely to be EHP, although still could not completely rule out the E-E within our current knowledge. Furthermore, in the case of electrical pumping, since the gain length is smaller and loss is larger than the optical pumping case, inevitably the injection carrier density should be even higher to overcome a larger threshold gain. As a result, the electrical driven lasing is dominated in EHP regime.

It is very difficult to estimate the current in a single nanowire. For example, n-ZnO nanowire/p-GaN LED devices show mA current in a large device scale, but the current in a single wire could not be estimated [18-19]. Here we present a very rough estimation. The threshold gain for optical pumping and electrical pumping in our device is calculated by using standard formula:

$$G_{th} = \frac{1}{2L}\ln\left(\frac{1}{R1 \times R2}\right)$$

$G_{th}=1.2\times10^4$ cm^{-1} for electrical pumping and $G_{th}=5.6\times10^3$ cm^{-1} for optical pumping are obtained due to different gain length and mirror reflectivity. In optical pumping, the pumped carrier density was estimated to be $\sim5.1\times10^{17}/cm^3$ (using 300 ps radiative recombination life time), so the carrier density needed in the electrical pumping should be

larger than $1\times10^{18}/cm^3$ with a reasonable assumption. Based on the similar formula for optical pumping, the relationship of current and carrier density in the electrical pumping case is: $n_p=I_{th}\tau/eV_{gain}$ where n_p is the carrier density, I_{th} is the threshold current, τ is the radiative recombination lifetime and V_{gain} is the volume of the gain region. V_{gain} is determined by the nanowire diameter (200 nm) and gain length (2.3 μm). Assuming τ=300 ps, I_{th} in each lasing nanowire is estimated to be 39 μA to 390 μA, corresponding to $1\times10^{18}/cm^3$ to $1\times10^{19}/cm^3$ carrier density.

The value of the estimated current in each lasing nanowire is reasonable due to the uneven distribution of current among the nanowires that are tightly connected with top ITO/glass contact. Initially this uneven current distribution may originate from the current crowding effect, very similar to the current crowding effect in those mesa-type LED devices, as evidenced by discrete lasing spots in both top-view and side-view optical images in previous chapter. Once the lasing is established in a certain number of wires, more electrons and holes will supply these nanowires than other spontaneously emitted nanowires to support the lasing modes. Further increase of injection current will make more nanowires with slightly different length to lase. Obviously, only a handful of active nanowires take part in the lasing under a certain injection current. It should noted that the threshold injection current in a single wire in this case is on the same order as that in CdS nanowire laser (200 μA) [13]. The ZnO nanowire laser diode gain/feedback schematic diagram is shown in Figure 7.2. The light experiences a gain for amplification in the p-n junction recombination region. Feedback and loss occur at the ZnO/substrate and ZnO/top electrode interface.

Because the device consists of a simple p-n junction, the gain region mainly includes the radiative recombination region. The width of this region is determined by both depletion region width and minority carrier diffusion length, i.e. electron diffusion length L_n and hole diffusion length L_p. A typical depletion width in ZnO p-n diode is < 100 nm considering that the doping levels in p-type and n-type are $10^{18}/cm^3$ and $10^{19}/cm^3$, respectively. The minority carrier diffusion length in p-ZnO is large, typically on the order of micron meters. In the earlier study by EBIC measurement [20], the electron diffusion length in highly Sb-doped p-type ZnO is about 2 μm. The L_p in n-type ZnO is much shorter, about 0.2 μm [21]. Thus the total gain region could be interpreted as 2.3 μm, as marked in orange in the figure.

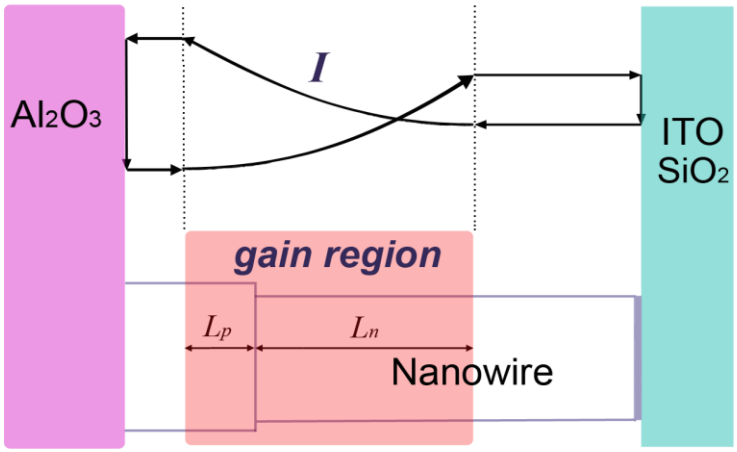

Figure 7.2 Schematic view of the gain/feedback in the device.

The bottom reflectivity is determined by the refractive index of sapphire substrate (n=1.65) and ZnO (n=2.5) to be 0.04. The top reflectivity is determined by three layers ZnO/ITO/glass (SiO_2). The refractive index ITO is 2.4 at 380 nm and glass has a refractive index of 1.45. Thus the total reflectivity at this side can be calculated to be

around 0.09.

Based on schematic structure of the device, the mirror loss can be deduced in a conventional way as:

$$G_{th} = \frac{1}{2L} \ln\left(\frac{1}{R1 \times R2}\right),$$

Where R1 is the reflectivity of ZnO/ITO/glass/air interface and R2 is the reflectivity of ZnO/Al_2O_3 interface. L is the gain length as 2.3 μm. This equation yields a threshold gain of about 1.2×10^4 cm^{-1}. This number seems to be high. Nevertheless, many ZnO nanostructure lasers (optical pumping) were demonstrated under similar configurations with threshold gain up to 1.7×10^4 cm^{-1} [27-36]. For a brief comparison, Huang *et al* [1] showed nanowire lasing under a threshold gain of 4.6×10^3 cm^{-1}, with a carrier density of $2\times10^{17}/cm^3$. Furthermore, FP type optically pumped lasing was demonstrated in our device (Figures 7.1), which proves that a carrier density of ~$5.1\times10^{17}/cm^3$ is enough to produce a threshold gain of 5.6×10^3 cm^{-1}. Therefore, it may be reasonable to sustain the threshold gain of 1.2×10^4 cm^{-1} if the device is operated under an order of magnitude higher carrier density.

Comparing this number with those reported in literature, we found that high threshold gain has been frequently observed in optically pumped ZnO nanostructures. Table 7.2 lists the reference papers that show FP and WGM type optically pumped lasing in ZnO nanostructures. Most lasers require gain larger than 10^4 cm^{-1} at room temperature.

Table 7.2 List of reference papers of ZnO nanostructure laser showing high threshold gain.

ZnO laser (type FP or WGM)	Size	Threshold gain (cm^{-1})	Temperature
Single Nanowire in air (FP) [22]	2.1 μm	7663	RT
Single Nanowire in air (FP) [23]	1.5 μm	10729	RT
Single Nanowire in air (FP) [24]	1.5 μm	10729	RT
Nanowire array on Si (FP) [25]	2 μm	12789	RT
Nanowire array on Si (FP) [26]	1.8 μm	14221	RT
Single Nanowire (FP) [27]	~1.4 μm	~11495	RT
Nanowire array on Si (FP) [28]	1.5 μm	17053	RT
Nanodisk (WGM) [29]	280 nm	~10000	RT
Nanowire array on GaN [30]	4.7 μm	12560	10 K
Single Nanowire in air [31]	1.5 μm	10729	Low temperature

On the other hand, considerable gain can be achieved in ZnO with low pumping density. For examples, Zhang *et al* [32] suggested that high-quality ZnO exhibits optical gain ~10 times higher than GaN based materials with same pumping intensity; Reynolds *et al* reported lasing in ZnO film with a pumping power as low as 10 W/cm^2 [33]; Huang *et al* [1] reported ZnO nanowire array lasing at 40 kW/cm^2, which leads to a carrier density of $2\times10^{17}/cm^3$. With this carrier density, 4.6×10^3 cm^{-1} threshold gain is produced as can be calculated using threshold gain equation. Vugt *et al* [22] reported ZnO single nanowire laser with a threshold pumping of 139 W/cm^2, which leads to a threshold carrier

density of only ~10^{16}/cm^3. The threshold gain is 5.0×10^3 cm^{-1}. These low carrier densities have already overcome the threshold gain on the order of 4×10^3 to 5×10^3 cm^{-1}, one to two orders of magnitude larger carrier densities through current injection is possible to generate enough gain to overcome 1.2×10^4 cm^{-1} threshold in the electrically pumped laser.

7.2 Gain Calculation of ZnO and Discussion

There is a lack of theoretical calculations for material gain in ZnO in electron hole plasma lasing scheme. Thus we performed a simple calculation. The result shows that at high pumping level 3.6x10^{19}/cm^3, it is possible to achieve threshold gain in our system.

Since our ZnO nanowires' diameters are in the scale of 200 nm, they can be treated as bulk when we do the calculation for the gain. The formula we used for the gain calculation is as follows:

$$\text{Gain}(\varepsilon) = \frac{\sqrt{2}\,(m_r)^{3/2}(qP_{cv})^2}{3\pi n_r \epsilon_0 m_0{}^2 (\hbar/2\pi)^2 c\varepsilon}(\varepsilon-\varepsilon_g)^{1/2}[f_n(\varepsilon_2)-f_p(\varepsilon_1)]$$

Where $\varepsilon_2 = \varepsilon_c + \frac{m_r}{m_e}(\varepsilon-\varepsilon_g)$

$$\varepsilon_1 = \varepsilon_v - \frac{m_r}{m_h}(\varepsilon-\varepsilon_g)$$

$\frac{2(P_{cv})^2}{m_0} = f_{cv} = 28.2$ ev ……oscillator strength of ZnO

The probability that a quantum state with energy ε_2 is occupied by an electron:

$$f_n(\varepsilon_2) = \frac{1}{1+\exp\left(\frac{\varepsilon_c+\frac{m_r}{m_e}(\varepsilon-\varepsilon_g)-\varepsilon_{fn}}{k_B T}\right)}$$

The probability that a quantum state with energy ε_1 is occupied by an electron:

$$f_p(\varepsilon_1) = \frac{1}{1+\exp\left(\frac{\varepsilon_v - \frac{m_r}{m_h}(\varepsilon - \varepsilon_g) - \varepsilon_{fp}}{k_B T}\right)}$$

Use the Joyce-Dioxn approximation:

$$\eta_c = \ln\left(\frac{n}{N_c}\right) + 2^{-3/2}\left(\frac{n}{N_c}\right)$$

$\varepsilon_{fn} = \varepsilon_c + \eta_c k_B T$ …….. quasi-Fermi level for electrons

$$\eta_v = \ln\left(\frac{p}{N_v}\right) + 2^{-3/2}\left(\frac{p}{N_v}\right)$$

$\varepsilon_{fp} = \varepsilon_v - \eta_v k_B T$ …… quasi-Fermi level for holes

η_c *and* η_v should be between -1 and 6, then the formulas are applicable.

$n \approx dn$

$p = p_0 + dp$

$dn = dp;$

dn *and* dp are the injection electron and hole concentration, respectively.

Reduced mass:

$$m_r = \frac{m_e m_h}{m_e + m_h}$$

Effective density of states in the conduction band:

$$N_c = \frac{2(2\pi m_e k_B T)^{3/2}}{h^3}$$

Effective density of states in the valence band:

$$N_v = \frac{2(2\pi m_h k_B T)^{3/2}}{h^3}$$

The list of constants:

m_0 = 9.11e-31 kg…….. rest mass of electron

$m_e = 0.28\ m_0$ …….DOS effective mass of electron

$m_h = 1.2\ m_0$ ……DOS effective mass of hole

p_0 = 2.5e18 cm^{-3}……hole concentration under equilibrium

$h = 6.626068 \times 10^{-34}\ m^2\ kg\ /\ s$ ….. Planck's constant

c = 2.99792e8…….speed of light in vacuum

q = 1.60218e-19 C……. elementary charge

$\epsilon_0 = 8.85 \times 10^{-12} F\ m^{-1}$ ……. Permittivity of vacuum

$\varepsilon_c = 3.3$ ev……. conduction band edge

$\varepsilon_v = 0$ ev ……...valence band edge

ε_g= 3.3 ev ……..bandgap energy of ZnO at 300K

$n_r = 2.4$ …….refractive index of ZnO

T = 300K……temperature

$k_B = 1.3806503 \times 10^{-23}\ m^2 kg\ s^{-2}\ K^{-1}$ …..Boltzmann constant

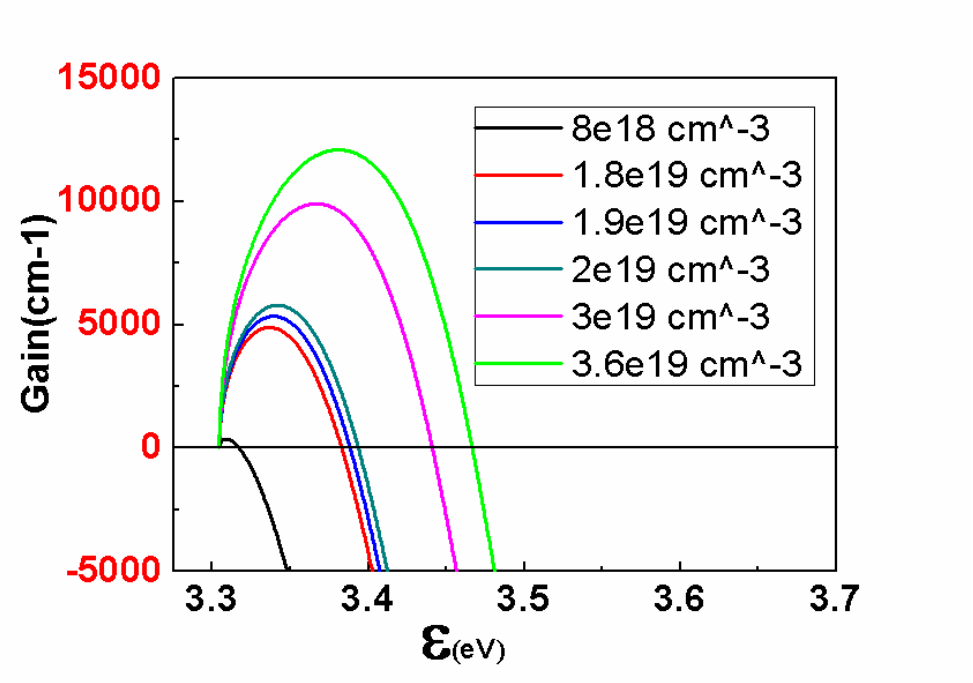

Figure 7.3 Gain spectra of the ZnO material under different injection concentration.

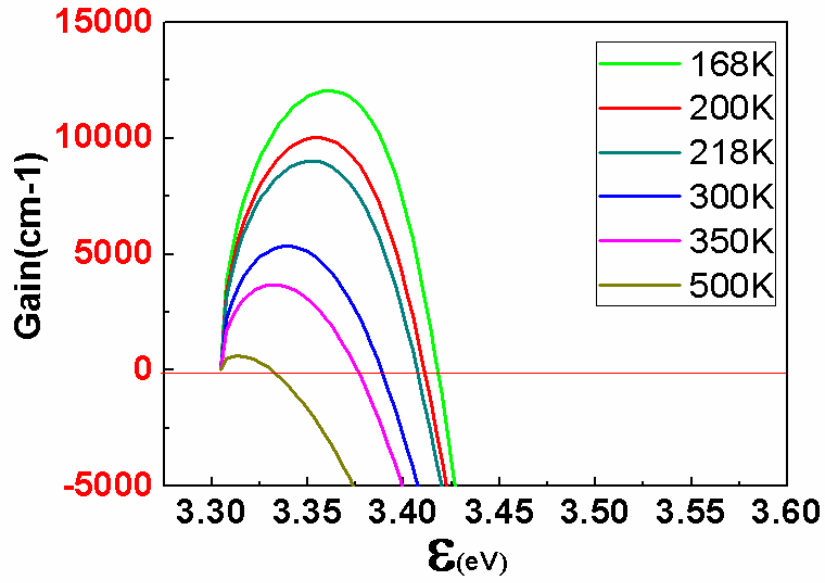

Figure 7.4 Gain spectra of the ZnO material under different temperature.

Fig.7.3 shows gain spectra of ZnO material under different injection concentration at room temperature. The gain increases as the increase of carrier density. Fig.7.4 shows gain spectra of ZnO material under different temperature with the same injection concentration of 1.8e19 cm^{-3}, the gain increases as the decrease of temperature.

In our case, the injection concentration in the nanowire is estimated to be 1.8e19 cm^{-3}. From the calculation result, when the injection concentration is 1.8e19 cm^{-3}, the maximum gain is around 5400 cm^{-1}, which is half of the threshold gain (12000 cm^{-1}). It seems the lasing can not happen. But from the previous analysis based on our experimental results and Table 7.2, we find ZnO nanostructure can overcome the high threshold gain usually on the order of 10000 cm^{-1}. So here we proposed some possible reasons:

Firstly, the end reflectivity: Because the diameter of the nanowires is usually smaller than the emitting light wavelength, the reflectivity for threshold gain equation may not be directly obtained by standard Fresnel equation that is applicable for the macroscopic case. Ning *et al* [34] and Wang *et al* [35] used FDTD method to numerically solve this problem in semiconductor nanowires. They found that the reflectivity strongly depends on the propagation modes and the nanowire diameter. At the nanowire/substrate interface, they suggested that the reflectivity can increase for about two to three times to about 0.1~0.2 and TE_{01} mode may dominate. The reflectivity between air and nanowire is larger and can be up to 0.7 for certain modes [36]. The enhanced end facet reflectivity may greatly reduce the threshold gain.

Secondly, actually the band structure of ZnO is still under controversy, so some

parameters of ZnO we used for the gain calculation including the density of states effective mass and the oscillator strength are not ideal. The “true” parameters maybe give rise to “the maximum gain values” matching the threshold gain.

7.3 Conclusion

In this chapter, nanowire lasing mechanism is discussed. EHP rather than excitonic lasing is responsible for our nanowire lasing. Furthermore, threshold gain spectra were calculated and future work is needed to completely understand the promising ZnO nanowire lasing.

7.4 References

1. M. H. Huang, S. Mao, & P. D. Yang et al, *Science* **8**, 1897 (2001).
2. H. Zhou, M. Wissinger, J. Fallert, R. Hauschild, F. Stelzl, C. Klingshirn, and H. Kalt. *Appl. Phys. Lett*. **91** 181112 (2007).
3. J. Dai, C. X. Xu, P. Wu, J. Y. Guo, Z. H. Li, Z. L. Shi, *Appl. Phys. Lett.* **97**, 011101 (2010).
4. K. Bando, T. Sawabe, K. Asaka, Y. Masumoto, *J. Lumin*. **108**, 385 (2004).
5. H. Y. Yang, S. P. Lau, S. F. Yu, A. P. Abiyasa, M. Tanemura, T. Okita, and H. Hatano, *Appl. Phys. Lett.* **89**, 011103 (2006).
6. C. Czekalla, C. Sturm, R. Schmidt-Grund, B. Cao, M. Lorenz, and M. Grundmann, *Appl. Phys. Lett.* **92**, 241102 (2008).
7. J. Fallert, R. J. B. Diez, H. Zhou, J. Sartor, C. Klingshirn, and H. Kalt, *Phys. Status.*

Solid. C **6**, 449 (2009).

8. B. Zou, R. Liu, F. Wang, A. Pan, L. Cao, and Z. L. Wang, *J. Phys. Chem. B* **110**, 12865 (2006).
9. Y. Ling, H. Cao, A. L. Burin, M. A. Ratner, X. Liu, and R. P. H. Chang, *Phys. Rev. A* **64**, 063808 (2001).
10. V. V. Ursaki, V. V. Zalamai, A. Burlacu, C. Klingshirn, E. Monaico, and I. M. Tiginyanu, 1.*Semicond. Sci. Technol.* **24**, 085017 (2009).
11. S. Gradecak, F. Qian, Y. Li, H. Park, and C. M. Lieber, *Appl. Phys. Lett.* **87** 173111 (2005).
12. C. Klingshirn, R. Hauschild, J. Fallert, and H. Kalt, *Phys. Rev. B*, **75**, 115203 (2007).
13. X. Duan, Y. Huang, R. Agarwal, and C. M. Lieber, *Nature* **421** 241(2003).
14. Y. F. Hsu, E. S. P. Leong, W. M. Kwok, A. B. Djurisic, S. F. Yu, D. L. Philips, W. K. Chan, *Opt. Mater.* **31**, 35 (2008).
15. A. N. Gruzintsev, A. N. Redkin, and C. Barthou, *Semiconductors* **44**, 628 (2010).
16. S. Chawla, K. Jayanthi, S. Singh, H. Chander, *J. Crystl. Growth* **310**, 3517 (2008).
17. Versteegh, M. A. M., Kuis, T., Stoof, H. T. C., Dijkhuis, J. I. *arXiv: 1012.3600* (2010).
18. X. M. Zhang, M. Y. Lu, Y. Zhang, L. Chen, and Z. L. Wang, *Adv. Mater.* **21**, 2767 (2009).
19. C. Chen, S. J. Chang, S. P. Chang, *Appl. Phys. Lett*. **95**, 223101 (2009).
20. O. Lopatiuk-Tirpak, L. Chernyak, *J. Appl. Phys*. **100**, 086101 (2006).
21. A. Soudi, P. Dhakal, and Y. Gu, *Appl. Phys. Lett*. **96**, 253115 (2010).
22. L. K. Van. Vugt, S. Ruhle, and D. Vanmaekelbergh, *Nano Lett*. **6**, 2707 (2006).

23. L. K. Van. Vugt, PHD thesis chapter 6, “Phase correlated non directional laser emission from ZnO nanowires.”

24. V. V. Ursaki, V. V. Zalamai, A. Burlacu, J. Fallert, C. Klingshirn, H. Kalt, G. A. Emelchenko, A. N. Redkin, A. N. Gruzintsev, E. V. Rusu, and I. M. Tiginyanu, *Superlattice Microst*. **46**, 513 (2009).

25. L. E. Greene, M. Law, J. Goldberger, F. Kim, J. C. Johnson, Y. Zhang, R. J. Saykally, and P. D. Yang, *Angew. Chem Int. Edit*. **42**, 3031 (2003).

26. S. Hirano, N. Takeuchi, S. Shimada, K. Masuya, K. Ibe, H. Tsunakawa, and M. Kuwabara, *J. Appl. Phys*. **98**, 094305 (2005).

27. W. M. Kwok, A. B. Djurisic, Y. H. Leung, W. K. Chan, and D. L. Phillips, *Appl. Phys. Lett.* **87**, 093108 (2005).

28. W. M. Kwok, A. B. Djurisic, Y. H. Leung, D. Li, K. H. Tam and D. L. Phillips, *Appl. Phys. Lett.* **89**, 183112 (2006).

29. D. J. Gargas, M. C. Moore, A. Ni, S. W. Chang, Z. Zhang, S. Chuang, and P. D. Yang, *ACS Nano* **4**, 3270 (2010).

30. H. Zhou, M. Wissinger, J. Fallert, R. Hauschild, F. Stelz, C. Klingshirn, and H. Kalt, *Appl. Phys. Lett*. 91 181112 (2007).

31. V. V. Zalamai, V. V. Ursaki, C. Klingshirn, H. Kalt, G. A. Emelchenko, A. N. Redkin, *Appl. Phys. B* 97 817 (2009).

32. X. Q. Zhang, Z. K. Tang, M. Kawasaki, A. Ohtomo, and H. Koinuma, *J. Cryst. Growth* **259**, 286 (2003).

33. D. C. Reynolds, D. C. Look and B. Jogai, *Solid State Commun*. **99**, 873 (1996).

34. A. V. Maslov and C. Z. Ning, *IEEE J. Quant. Electron* **40**, 1389 (2004).

35. S. Wang, Z. Hu, H. Yu, W. Fang, M. Qiu, L. Tong, *Optics Express* **17**, 10881 (2009).

36. A. Henneghien, B. Gayral, Y. Desieres, and J. M. Gerard, *J. Opt. Soc. Am. B* **26**, 2396 (2009).

Chapter Eight Conclusions

(1) A simple way was demonstrated to make the flexible DSSC based on the transfer of a large scale array of highly oriented vertical ZnO nanowires. The large shunt resistance of the DSSC, which greatly benefits from the intactness of the transferred nanowire array, results in a good fill factor. The resulting DSSC on flexible substrate achieved a prominent photovoltaic effect even if the device was operated under severe bending condition, which is very promising for future flexible optoelectronics application.

(2) Ag-doped ZnO nanowires were grown via CVD process. The PL spectrum of the Ag-doped nanowires shows an Ag-related peak at 3.328 eV at 14 K, which can be attributed to neutral-acceptor-bound excitons (A^0X). Temperature- and excitation power-dependent PL spectra confirm shallow acceptor level of 0.158 eV. The electrical measurement results suggest that the conductivity of Ag-doped ZnO nanowires is *p*-type and the hole mobility is approximately 0.18 $cm^2 V^{-1} S^{-1}$. After 5 months, however, originally p-type Ag-doped ZnO nanowires turned into n-type judging from NWFET measurements. Therefore, long-term p-type stability of Ag-doped ZnO nanowires is still an issue. The shallow-acceptor induced energy level of the Sb-doped ZnO nanowire array is observed by low-temperature PL at 3.350 eV.

(3) ZnO p-n homojunctions based on Sb-doped p-type nanowire arrays and n-type thin films were grown by the combination of CVD and MBE. The ZnO thin film/nanowire p-n junction was proved by EBIC profiling, I-V measurement, and field-effect measurement. Evident photoresponse was observed in the UV region of the PC spectra. This study not only proved that Sb doping can lead to p-type ZnO nanowires but also demonstrated an ultraviolet homojunction photodetector device based on p-type nanowire array and n-type thin film.

(4) ZnO p-n homojunctions based on Sb-doped p-type nanowire arrays and n-type thin films were grown by the combination of CVD and MBE. Evident UV emissions were observed under different current injection. This study not only proved that Sb doping can lead to p-type ZnO nanowires but also demonstrated an ultraviolet homojunction LEDs based on p-type nanowire array and n-type thin film.

(5) The electrically pumped ZnO nanowire diode lasers using *p*-type Sb-doped ZnO nanowires and *n*-type ZnO film were achieved. FP type UV lasing was demonstrated at RT with good stability. The work on ZnO UV lasing may enable many potential applications. Future work is needed to further optimize the laser performance. For examples, the top contact with the *p*-type nanowire might be engineered to offer both good optical transparency and low electrical resistivity;

Heterojunction nanowire diode structures may be used to achieve stronger power output.

(6) Nanowire lasing mechanism is discussed. EHP rather than excitonic lasing is responsible for our nanowire lasing. Furthermore, threshold gain spectra were calculated and future work is needed to completely understand the promising ZnO nanowire lasing.